Master Thesis

MSc in Automotive Engineering MSc in Mechanical Engineering

Drag Torque and Synchronization Modelling in a Dual Clutch Transmission

CHINA EURO VEHICLE TECHNOLOGY AB

June 12, 2018

Keerthi Medleri Hire Math
medleri@student.chalmers.se

Mikael Lund
mikael.a.lund@outlook.com

CHALMERS
UNIVERSITY OF TECHNOLOGY

Department of Mechanics and Maritime Sciences
CHALMERS UNIVERSITY OF TECHNOLOGY

LUNDS
UNIVERSITET

Department of Mechanical Engineering
LUND UNIVERSITY

Gothenburg, Sweden

Preface

This paper has been written in order for the authors to receive Master of Science titles from Lunds Tekniska Högskola and Chalmers respectively. Both authors have been contributing equally to all parts of the thesis. It has been written in collaboration with CEVT AB located at Lindholmen in Gothenburg, Sweden. The authors want to thank the supervisors Anette Andersson and Sven Andersson for their support before and during this thesis. We also want to thank our supervisor at CEVT, Eva Barrientos Blanco, as well as Henrique Budacs, Viktor Pettersson and all other people at CEVT for answering all our questions.

Abstract

Noise, vibration and harshness (NVH) is a big consideration in the automotive industry. In order to create an as pleasant driving experience as possible for the driver, NVH should be minimized. One of the sources of NVH comes from the transmission due to the synchronization process. When shifting between gears, the speeds of the target gear and the output shaft it is supported by, have to be synchronized. This is achieved through synchronization rings that, through friction, synchronize the speeds of the components before engaging them to each other. However, there is a torque, the gearbox's drag torque, that can interfere with this process by slowing down the input shaft. This drag torque therefore aids the synchronization process during an up-shift and resists it during a down-shift. Today's automotive industry lacks a definite method to calculate this drag torque and as a result, values are assumed to simplify the problem.

This thesis has provided a model that calculates the drag torque at different operating conditions depending on input speed, input torque, temperature and other variables. The drag torque comes from several different sources in a transmission and can be separated into load dependent and speed dependent drag torque. The sources include viscous shear in the clutch, gears churning in an oil bath, gear windage in an air-oil mist, bearing rolling elements churning in oil, friction in bearings, friction in gear meshes, pocketing (also called squeezing) of oil between surfaces in gear meshes and viscous shear between concentric shafts. The load dependent are those which are generated through friction, i.e. the friction in bearings and gear meshes. Speed dependent are those generated through resistance from a surrounding medium.

This thesis has developed multiple models within each source of drag torque and summed them up for a total drag torque. The results have been compared to test data to verify which combination of models from each source of drag torque sums up to a reliable result. The thesis also shows big differences between different models, but manages to acquire a combination of models that lies relatively close to the test results.

The thesis has further used the new drag torque model to evaluate the friction lining on the existing synchronizer rings of a particular transmission to see if the design is appropriate. It also analyzes how a different inertia in the gearbox influences the maximum speed the synchronizers are able to synchronize. Here, it is found that only frictional work and the slip time are influenced of the investigated parameters; specific frictional work, slip time, pressure, slip speed and specific frictional power.

Keywords: drag torque, synchronization, dual clutch transmission

Contents

List of Figures

List of Tables

Nomenclature

Term	Description	Unit	Term	Description	Unit
		General			
n	Rotational speed	rpm	ω	Rotational speed	rad/s
μ	Coefficient of friction	-	g	Acceleration due to gravity	m/s^2
t	Time	s	$\Delta\omega$	Speed difference	rad/s
V_0	Volume of oil reserve	m^3			
		Drag torque			
$T_{drag,clutch}$	Total clutch drag torque	Nm	$T_{drag,bearing}$	Total bearing drag torque	Nm
$T_{drag,churn}$	Total churning drag torque	Nm	$T_{drag,windage}$	Total windage drag torque	Nm
$T_{drag,shafts}$	concentric shaft drag torque	Nm	$T_{drag,pocketing}$	Pocketing/squeezing drag torque	Nm
$T_{drag,gear}$	Total Gear mesh drag torque	Nm			
		Clutch			
R_o	Clutch disc outer radius	m	u_r	Radial velocity	m/s
R_i	Clutch disc inner radius	m	u_θ	Circumferential velocity	m/s
R_*	Clutch disc effective radius	m	u_z	Axial velocity	m/s
Q_a	Actual oil flow rate	m^3/s	Q_c	Centrifugal force-induced flow rate	m^3/s
Q_r	Required oil flow rate	m^3/s			
T_{ff}	Clutch drag torque due to continuous oil film	Nm	T_{rf}	Clutch drag torque due to ruptured oil film	Nm
T_{mf}	Clutch drag torque due to oil-mist film	Nm	h	Clutch gap between friction discs	m
Re	Reynold's number	-	Fr	Froude's number	-
P_a	Ambient pressure	N/m^2	Δp	Pressure difference between oil inside clutch and surroundings	N/m^2
R_m	Clutch mean radius	m	p	Pressure	Pa
n_i	Number of friction pairs	$-$			
A_{ng}	Non-grooved clutch area	m^2	A_{tot}	Total friction disc area	m^2

Gears

T_{in}	Input torque	Nm	i	Gear ratio	-
α	Pressure angle	$^\circ$	β	Helix angle	$^\circ$
r_p	Gear pitch radius	m	d_p	Gear pitch diameter	m
ϵ	Addendum contact ratio	-	z	Number of gear teeth	-
f_g	Gear dip coefficient	-	b	Gear face width	m
d_r	Root diameter	m	h_{tooth}	Gear tooth height	m
$d_{o,s}$	Outside diameter of shaft	m	l_s	Length of shaft	m
R_f	Gear roughness factor	-	h_{imm}	Gear immersion depth in oil	m
H_v	Drag loss factor	-	ϵ_α	Gear profile contact ratio	-
V_s	Sliding velocity of gear	m/s	V_r	Rolling velocity of gear	m/s
v_t	Gear tangential velocity	m/s	d_m	Gear mean diameter	m
r_o	Gear outer radius	m	r_i	Gear inner radius	m
d_o	Gear outer diameter	m	X_L	Lubrication factor	-
m_n	Gear normal module	$-$	m_t	Gear transverse module	$-$
ρ_c	Gear-pair equivalent curvature	m			

Subscripts: 1-Input gear; 2-Output gear

Bearings

$d_{b,i}$	Bearing bore diameter	mm	$d_{b,o}$	Bearing outer diameter	mm
$d_{b,m}$	Bearing mean diameter	mm	$h_{b,imm}$	Bearing immersion level	mm
i_{rw}	Amount of ball-bearing rows	-	K_{rs}	Replenishment/starvation factor	-
T_{rr}	Bearing rolling friction torque	Nm	T_{sl}	Bearing sliding friction torque	Nm
T_{seal}	Bearing seal friction torque	Nm	$T_{b,drag}$	Bearing lubrication loss	Nm
T_{BLDA}	Axial load-dependent bearing drag	Nm	T_{BLDR}	Radial load-dependent bearing drag	Nm
T_{BSD}	Speed-dependent bearing drag	Nm			
ϕ_{ish}	Inlet shearing reduction factor	-	ϕ_{rs}	Kinematic replenishment/starvation factor	-
ϕ_{bl}	Bearing weighting factor	-	f_2	Bearing coefficient	-
G_{rr}	Bearing load-dependent variable	-	G_{sl}	Bearing load-dependent variable	-
C	Bearing load rating	kN	$b_{bearing}$	Bearing width	mm
K_{S1}	Bearing constant	Nmm	K_{S2}	Bearing constant	Nmm
μ_{sl}	Sliding friction coefficient	-	μ_{bl}	Bearing lubricant factor	-
μ_{EHL}	Sliding friction coefficient in full film condition	-	β_{seal}	Bearing seal constant	-
d_{seal}	Seal counter-face diameter	mm	V_M	Bearing drag loss factor	-
f_0	Bearing coefficient	-	f_1	Bearing coefficient	-
P_1	Bearing equivalent radial load	N	F_a	Bearing axial load	N

Oil

ν_{kin}	Oil kinematic viscosity	mm^2/s	ν_{dyn}	Oil dynamic viscosity	Pas
$\nu_{dyn,mist}$	Oil-mist dynamic viscosity	Pas	ρ	Oil density	kg/m^3

Synchronizer

n_c	Number of cones	$-$	Δt	Synchronizer slip time	s
$T_{s,z}$	Synchronizer Indexing torque	Nm	$T_{s,f}$	Synchronizer friction torque	Nm
$d_{s,m}$	Synchronizer mean diameter	m	$d_{s,p}$	Synchronizer pitch diameter	m
P_m	Mean friction power	W	P_{mA}	Specific mean frictional power	W/m^2
W	Frictional work	J	q_A	Specific frictional work	J/m^2
$d_{s,max}$	Maximum Synchronizer diameter	m	J	Inertia	kg/m^2
p_m	Synchronizing pressure	Pa	$v_{s,max}$	Maximum synchronizer slip speed	m/s
$F_{s,N}$	Synchronizer normal force	N	A_s	Friction lining area	m^2
P_{max}	Maximum friction power	W	ψ	Roof angle	$^\circ$
μ_{cones}	Friction coefficient of friction lining	$-$	μ_d	Friction coefficient between roofs	$-$
φ	Cone angle	$^\circ$	F_a	Axial force	N

Note: The units are as in the tables unless otherwise specified.

1 Introduction

1.1 Background

Synchronizers in a gearbox allow smooth gearshifts in a noiseless and vibration-free manner which improves the durability of the transmission and gives better comfort to the driver. This is achieved by reducing the rotational speed difference between the gear and the shaft it sits on when shifting [2]. Although the synchronizers produce smooth gear-shifts, they are sensitive to drag torque generated throughout the transmission [32]. When synchronization is complete and no frictional torque exists between the synchronizer and gear, the drag torque can reintroduce a relative speed. Hence, it is important to investigate the effect of drag torque on the overall performance of the transmission. For this purpose, mathematical models concerning the drag torque of a dual clutch transmission and its effect on synchronizers are developed in this project. Currently, this drag torque is given an assumed value. An added advantage to developing the models is the reduced time and efforts through virtual simulations in comparison with experiments. Previously, a detailed approach to the different drag torque losses involved in a dual clutch transmission has been conducted by Walker et al. [37].

1.2 Aim

To develop mathematical models to estimate the drag torque in a dual clutch transmission and evaluate the synchronizers' capability for multiple gear-shift scenarios and different inertias.

1.3 Focus and delimitations

The thesis is time-limited to 20 weeks. It is also limited through the fact that no single source of drag torque can be verified alone and the test data only exists for the complete gearbox. The focus of the thesis is to give a basic understanding of drag torque in a gearbox, evaluate its influence on synchronizers and what work needs to be done in order to advance within the subject.

1.4 Methodology

A model for calculating the drag torque in a specific dual clutch transmission was created in MATLAB/Simulink. All the required input data was provided by CEVT according to a gearbox. The model was divided into sub-models, one for each source of drag torque, which were then transferred to the input shaft and summed up for a total drag torque, as the experimental data contains the drag torque determined at the input shaft. Most sources of drag torque have several different models to gain the possibility of comparing different models and to find the best combination of different sources that complies with the experimental data. When the computational model was completed, it was verified towards test data provided by CEVT. This model was then used to improve an already existing model of the synchronization process in the gearbox.

When evaluating the synchronizers, the model was slightly altered. Only the drag torque experienced by the synchronizer being evaluated, and not the engine, was used. The synchronizer ring was evaluated for both the highest and the lowest axial force that the gear actuator can provide. Once the synchronizers have been evaluated for the current state, they were evaluated with respect to how many revolutions per minute they can synchronize when there is a change of inertia, due to change a of components within the transmission, while still being within specifications.

All results are normalized due to a confidentiality requirement from CEVT.

2 Theory

2.1 Synchronization

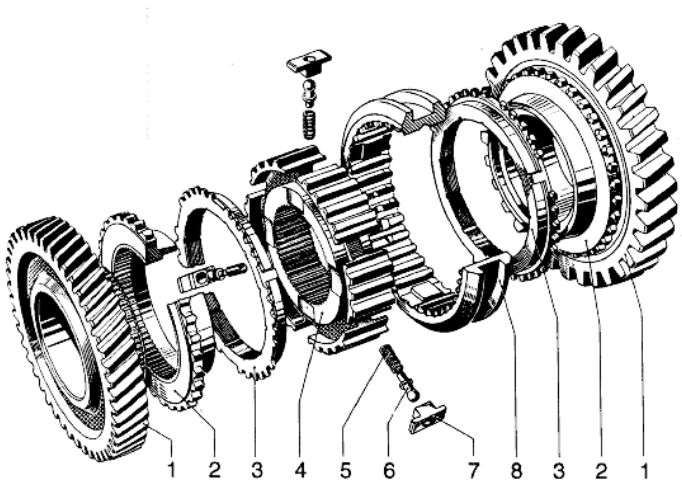

Figure 1: Exploded view of a synchronized gear-mesh, [20]

In figure 1, the different parts that make up for a synchronized gear mesh can be identified. Part (1) is the gear that is meshing with a pinion on the input shaft (not seen). This gear is supported by a bearing on a output shaft going through all parts in the figure (shaft not seen), and can therefore have a relative speed with respect to the shaft that supports it. Part (2) is the dog ring that is solidly connected to the gear (1). The dog ring has teeth and a tapered cone that will interact with the synchronizer ring, (3), in a way explained further down. Number (4) is the hub which is solidly connected to the output shaft. It is through the hub that the torque will be transmitted from the shaft to the gear-mesh. Parts (5-7) are a spring, pinball and a thrust piece respectively that keep the sleeve (8) in neutral. The sleeve pushes the synchronizer ring towards the dog-ring via the thrust piece. When shifting gears in a manual transmission, it is the sleeve that is moved when the driver shifts the gear-lever [20].

Lechner and Naunheimer [20] splits up the synchronization process into 5 phases, I-V, see figure 2. Before phase I starts, the sleeve is held in the middle of the hub by the pin ball. As the gear shift process starts, a mechanism inserts an axial force, F_a, on the sleeve to push it axially towards the gear to be synchronized. This pushes the synchronizer ring's counter-taper against the taper on the dog-ring. Since there is a speed difference between the sleeve and synchronizer ring relative to the dog-ring, the synchronizer ring rotates slightly relative to the sleeve until the roofs of their dogs engage, phase I, also called asynchronization, ends.
The main synchronization, phase II, starts. Now there is a frictional torque, T_f (often denoted as taper torque, T_C or T_R), and a gearing torque, T_Z (often denoted as blocking release torque or indexing torque T_I). The gearing torque acts as if to open the mechanism while the frictional torque acts as to close the mechanism, i.e. T_f pushes the dogs of the synchronizer ring into the dogs of the sleeve while T_Z tries to separate the contact. While there is a relative speed in the frictional lining, the frictional torque is greater than the gearing torque and the sleeve cannot move. When the relative speed has reached zero, phase II is concluded and phase III, the unlocking (or blocking release), starts.
As there is no relative speed any longer, the frictional torque goes towards zero. This allows the gearing

torque to rotate the synchronizer ring slightly relative to the sleeve. The sleeve then enters free flight and moves axially until it makes contact with the dog-ring.
In phase IV, the turning, a new gearing index is generated by the contact between the dogs of the sleeve and the dogs of the dog-ring. Since there is no relative speed there is no frictional moment. The gearing torque can turn the dog-ring relative to the sleeve. The sleeve can then fully engage the gear and allow power flow, phase V.

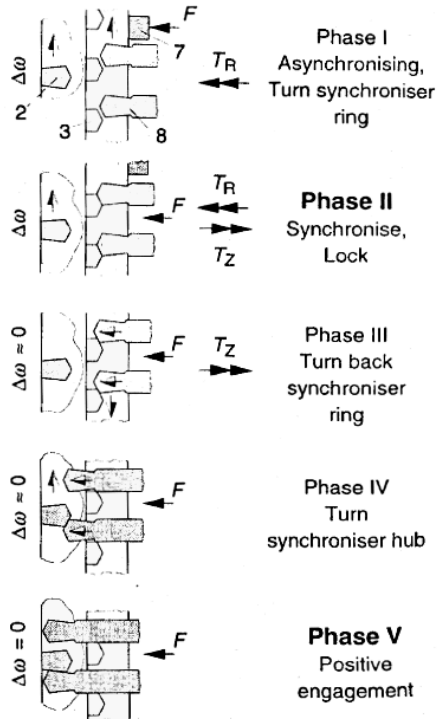

Figure 2: Synchronization phases, [20]

According to Lechner and Naunheimer [20], drag torque can reintroduce a relative speed after phase II (see section 2.1) if it is too big. This can cause grating as the dogs repeatedly come in and out of contact. Since the drag torque tries to slow down the gear, it aids the synchronization (phase II) during up-shift and resists it during down-shift. This can affect the friction lining in the synchronizer ring and hence the drag torque needs to evaluated in detail.

2.2 Drag torque

Walker et al. [41] states that drag torque in a transmission is the torque losses that originate from different sources within the transmission, and is obtained by dividing the power losses from each source with the rotational speed. The drag torque is broadly classified into two types:

- Load-dependent drag torque
- Speed-dependent drag torque

where, load-dependent drag torque originates due to sliding and rolling friction between mechanical components in the transmission and speed-dependent drag torque originates due to the media (lubri-

cants, air) interaction with the components inside the transmission. The sources of torque loss are further classified based on the type of drag torque:

- Speed-dependent drag torque
    1. Bearings
    2. Clutch
    3. Churning
    4. Concentric shaft shear
    5. Windage
    6. Pocketing
- Load-dependent drag torque
    1. Bearings
    2. Gear mesh

The theory behind each of the source of drag torque is explained in the following section followed by the results in section 3.

2.2.1 Bearings

According to Schlegel et al.[29], bearings contribute to the resistance in a gearbox through sliding and rolling friction, seal friction and lubrication losses.

Since a bearing has both load-dependent and speed-dependent losses, a bearing which is not under load will generate a drag torque. When analyzing a bearing which supports a gear driven by the same input shaft as the separate engaged gear, it is not known how the drag torque is split up. One part of the drag torque flows through the gear the bearing supports, another part flows through the engaged gear via the output-shaft. Therefore, the drag torque cannot simply be multiplied with the ratio of the engaged gear in order to be transferred to the input shaft. Instead, the concept of power is used, all lost power must come from the input. Therefore, by calculating the power loss and dividing by the input rotational speed, the drag torque at the input can be calculated.

2.2.1.1 SKF bearing model

According to SKF [27], the SKF-model is an approximation of advanced computational methods developed by SKF. The frictional moment in a bearing can be divided into three zones, see figure 3. In the first zone, the start-up period, the drag torque decreases due to a full lubrication film being formed when viscosity or rotational speed increases. In the second zone, a full film exists and its thickness increases which also increases frictional moment. In zone three, there is a kinematic starvation and inlet shear which causes the drag torque to plateau.

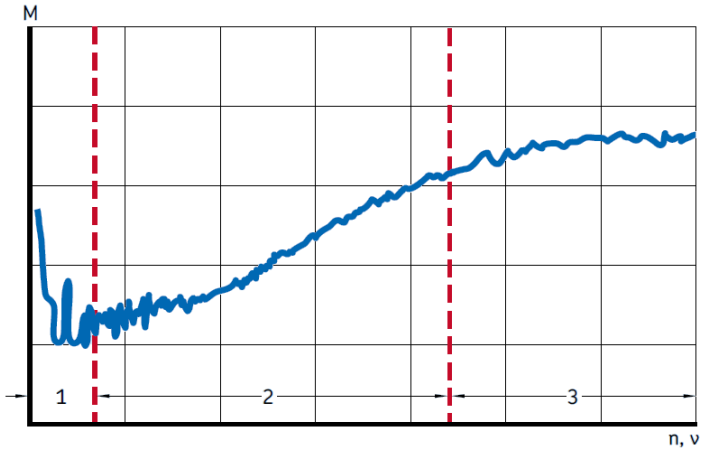

Figure 3: Bearing drag torque versus viscosity and rotational speed, [27]

These factors are considered with an *Inlet shear heating reduction factor* and a *Kinematic replenishment/reduction factor*. According to SKF [27], the following sources and their tribological effect have to be considered in order to accurately calculate the drag torque:

- the rolling frictional moment and eventual effects of high-speed starvation and inlet shear heating
- the sliding frictional moment and its effect on the quality of the lubrication
- the frictional moment from seal(s)
- the frictional moment from drag losses, churning, splashing etc.

The SKF model works by summarizing losses from different sources into one total drag torque:

$$T_{drag,bearing} = T_{rr} + T_{sl} + T_{seal} + T_{b,drag} \tag{1}$$

where all torques are given in Nmm. The method has some conditions that need to be fulfilled:

- Kinematic viscosity ranges from 2 to 500 mm^2/s
- Loads equal to or larger than minimum recommended load and at least:
  - 0,01C for ball bearing
  - 0,02C for roller bearings
- Constant load in magnitude and direction
- Normal operating clearance in the bearings
- Constant speed not higher than permissible speed

2.2.1.1.1 Rolling frictional moment

The SKF-model calculates the rolling frictional moment through:

$$T_{rr} = \phi_{ish}\phi_{rs}G_{rr}(n\nu_{kin})^{0,6} \tag{2}$$

where the rolling frictional moment is given in Nmm, n is the rotatiol speed in rpm and G_{rr} is a variable depending on:

- bearing type

- bearing mean diameter
- radial load
- axial load

Method for calculating G_{rr} is provided in the catalogue.

Inlet shear heating reduction factor
According to SKF [27], only a small amount of the lubricant available inside the bearing can come between the rolling element and the ring in order to create a film. Some of the flow is pushed away and produces a reversed flow, see figure 4. This flow shears the fluid, generating heat and therefore lowering viscosity. This reduces the film thickness and therefore rolling friction. The model provides an estimation of this factor:

$$\phi_{ish} = \frac{1}{1 + 1,84 * 10^{-}9(nd_{b,m}^{1,28}\nu_{kin}^{0,64})} \tag{3}$$

where $d_{b,m}$ is the mean diameter of the bearing given by:

$$d_{b,m} = \frac{d_{b,i} + d_{b,o}}{2} \tag{4}$$

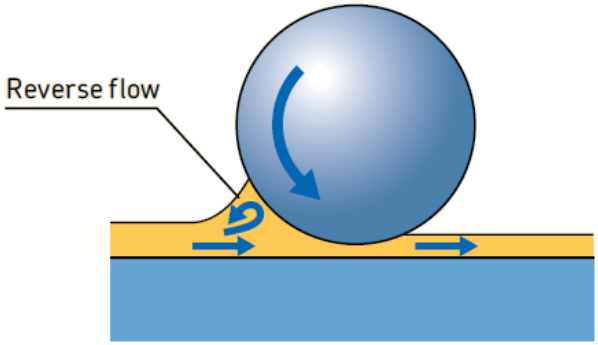

Figure 4: Reverse flow in a bearing, [27]

Kinematic replenishment/starvation reduction factor
In certain conditions, the lubrication does not have enough time to flow back to the contact surface between rolling element and ring in the bearing. This reduces the thickness of the film and therefore the rolling friction. This occurs if the bearing is submerged in a bath while viscosity or speed is high. The model provides an estimation of this factor:

$$\phi_{rs} = \frac{1}{e^{K_{rs}\nu_{kin}n(d_{b,i}+d_{b,o})\sqrt{\frac{K_z}{2(d_{b,o}-d_{b,i})}}}} \tag{5}$$

where e is the base of the natural logarithm, K_{rs} is a replenishment/starvation constant which is equal to:

- $3 * 10^{-8}$ for low level oil baths and oil jet lubrication
- $6 * 10^{-8}$ for grease and oil/air lubrication

and K_z is a constant related to bearing geometry and type found in the catalogue.

2.2.1.1.2 Sliding frictional moment

According to the SKF-model [27], the sliding frictional moment can be calculated:

$$T_{sl} = G_{sl}\mu_{sl} \tag{6}$$

where G_{sl} is a variable dependent on:

- bearing type
- bearing mean diameter
- radial load
- axial load

Method for calculating G_{sl} is provided in the catalogue. The sliding frictional coefficient is depending on if there is a full film or not:

$$\mu_{sl} = \phi_{bl}\mu_{bl} + (1 - \phi_{bl})\mu_{EHL} \tag{7}$$

where ϕ_{bl} is a weighing factor between full film lubrication and no film:

$$\phi_{bl} = \frac{1}{e^{2{,}6*10^{-8}(n\nu_{kin})^{1,4}d_{b,m}}} \tag{8}$$

μ_{bl} is a factor depending on additives in the lubrication. SKF states that this is generally around 0,15. The sliding frictional coefficient in full film conditions, μ_{EHL}, is equal to:

- 0,02 for cylindrical roller bearings
- 0,002 for tapered roller bearings
- 0,05 for other bearings lubricated with mineral oil
- 0,04 for other bearings lubricated with synthetic oil
- 0,1 for other bearings lubricated with transmission fluid

2.2.1.1.3 Frictional moment from seal

According to SKF [27], the frictional moment from seals can sometimes be greater than those from the bearing itself and should therefore not be ignored. The moment can be estimated through:

$$T_{seal} = K_{S1}d_{seal}^{\beta_{seal}} + K_{S2} \tag{9}$$

where K_{S1}, β_{seal} and K_{S2} are are given from tables in the catalogue. K_{S1} is a constant dependent on:

- seal type
- bearing type and size

β_{seal} is a constant depending on:

- seal type
- bearing type

and K_{S2} is a constant dependent on:

- seal type
- bearing type and size

It should be noted that equation 9 provides the frictional moment from both seals and should be divided by a factor of two if only one seal exists.

2.2.1.1.4 Lubrication losses

According to SKF [27], bearings rotating in oil bath contribute to resisting moment that should not be neglected. It is also affected by various factors other than oil viscosity and rotational speed such as size and geometry of the oil reservoir and oil agitation from close by mechanical elements such as gears and cams. The SKF-model, however, neglects the effects from the properties of the oil reservoir and fluid agitation. Following conditions apply to the model:

- Effects from oil reservoir size and geometry and from oil agitation is negligible
- Shaft is horizontal
- Constant rotational speed not higher than permissible speed
- Kinematic viscosity below
  - $\leq 500mm^2/s$ when bearing is submerged half or less
  - $\leq 250mm^2/s$ when bearing is submerged more than half

The resisting moment from drag for ball bearings is estimated from:

$$T_{b,drag} = 0,4V_M K_{ball} d_{b,m}^5 n^2 + 1,093 * 10^{-7} n^2 d_{b,m}^3 \left(\frac{n d_{b,m}^2 f_t}{\nu_{kin}} \right)^{-1,379} R_s \tag{10}$$

The resisting moment from drag for roller bearings is estimated from:

$$T_{b,drag} = 4V_M K_{roll} C_W b_{bearing} d_{b,m}^4 n^2 + 1,093 * 10^{-7} n^2 d_{b,m}^3 \left(\frac{n d_{b,m}^2 f_t}{\nu_{kin}} \right)^{-1,379} R_s \tag{11}$$

where K_{ball} and K_{roll}:

$$K_{ball} = \frac{i_{rw} K_z (d_{b,i} + d_{b,o})}{d_{b,o} - d_{b,i}} 10^{-12} \tag{12}$$

$$K_{roll} = \frac{K_L K_z (d_{b,i} + d_{b,o})}{d_{b,o} - d_{b,i}} 10^{-12} \tag{13}$$

The variables and constants for calculations of drag losses are:

$$C_w = 2,789 * 10^{-10} l_d^3 - 2,786 * 10^{-4} l_d^2 + 0,0195 l_d + 0,6439 \tag{14}$$

$$l_d = 5 \frac{K_L b_{bearing}}{d_{b,m}} \tag{15}$$

$$f_t = \begin{cases} \sin(0,5t), & \text{when } 0 \leq t \leq \pi \\ 1, & \text{when } \pi < t < 2\pi \end{cases} \tag{16}$$

$$R_s = 0,36 d_{b,m}^2 (t - \sin t) f_A \tag{17}$$

$$t = 2 \arccos \frac{0,6 d_{b,m} - h_{b,imm}}{0,6 d_{b,m}}, \quad when \;\; h_{b,imm} > 1,2 d_{b,m}, use \;\; h_{b,imm} = 1,2 d_{b,m} \tag{18}$$

$$f_A = 0,05 \frac{K_z (d_{b,o} + d_{b,i})}{d_{b,o} - d_{b,i}} \tag{19}$$

where the drag loss factor, V_M, is according to diagram in figure 5, $h_{b,imm}$ is oil level according to figure 6, i_{rw} are number of rows of rolling elements and K_L is a roller bearing type related geometric constant from the catalogue.

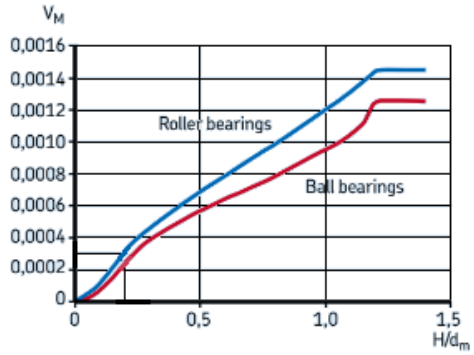

Figure 5: Drag loss factor for SKF bearings, [27]

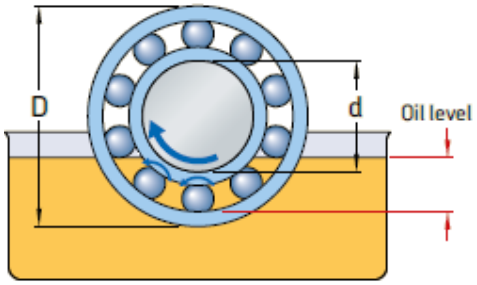

Figure 6: Oil level for a bearing, [27]

2.2.1.2 ISO bearing model

An approach associated to the drag torque losses in bearings has also been developed by International Organization for Standardization [11]. However, the coefficients used in the model is only referring to SKF-bearings.

The different drag losses associated with bearings are divided into two categories: load-dependent and speed-dependent losses, each of which are explained in sections 2.2.1.2.1 and 2.2.1.2.2. The total drag torque originating from the bearings is according to:

$$T_{drag,bearing} = T_{BLDA} + T_{BLDR} + T_{BSD} \tag{20}$$

2.2.1.2.1 Load-dependent losses

The load-dependent losses originate due to mechanical friction present between two surfaces, sliding and rolling. The radial load-dependent drag torque in bearing follows equation 21 while the axial load-dependent drag torque in bearings follows the equation 22:

$$T_{BLDR} = \frac{f_1 \cdot {P_1}^a \cdot {d_{b,m}}^b}{1000} \tag{21}$$

$$T_{BLDA} = \frac{f_2 \cdot F_a \cdot d_{b,m}}{1000} \tag{22}$$

where, a and b are modifiers depending on the series of bearings being used. They exist in the standard.

2.2.1.2.2 Speed-dependent losses

The speed-dependent losses are losses that originate due to the presence of media (air and lubricant) and are affected by the type and properties of lubricants used in the system and the rotating speed of the bearings. The relation to determine the speed-dependent bearing losses is according to:

$$T_{BSD} = \begin{cases} 1.6 \cdot 10^{-8} \cdot f_0 \cdot {d_{b,m}}^3 & \text{if } \nu_{kin} \cdot n < 2000 \\ 10^{-10} \cdot f_0 \cdot (\nu_{kin} \cdot n)^{2/3} \cdot {d_{b,m}}^3 & \text{if } \nu_{kin} \cdot n \geq 2000 \end{cases} \tag{23}$$

2.2.1.3 Schaeffler bearing model

Schaeffler Technologies has developed an empirical model to estimate the power loss from bearings which are slightly different from that of the ISO model, explained in section 2.2.1.2. This model is however only applicable only to the bearings manufactured by Schaeffler [28].

Just like the other models, the power loss, or rather drag torque, is decomposed into two parts: load-dependent drag torque and speed-dependent drag torque. Therefore, the total drag torque from Schaeffler bearings is given by equation 24:

$$T_{drag,bearing} = T_{drag,load} + T_{drag,speed} \tag{24}$$

where, $T_{drag,load}$ is the bearing load dependent drag torque and $T_{drag,speed}$ is the bearing speed dependent drag torque.

The bearing speed-dependent drag torque for Schaeffler bearings is the same as that used by the ISO model which is given by the equation 23. However, the bearing coefficient f_0 is determined from the specific tables in Schaeffler bearing catalogue [28].

The bearing load dependent drag torque as the name suggests is dependent on the radial and axial loads that act upon the bearings, both static and dynamic. The drag torque is given by empirical equations that are different for the type of bearings as seen in equations 25 and 26.

- For needle roller and cylindrical roller bearings:

$$T_{drag,load} = f_1 \cdot F \cdot d_{b,m} \tag{25}$$

- For tapered roller bearings and spherical roller bearings:

$$T_{drag,load} = f_1 \cdot P_1 \cdot d_{b,m} \tag{26}$$

2.2.1.4 Hybrid model

Since there are manufacturer-specific models, a hybrid model is made. This model simply uses the SKF-model for the SKF-bearings and the Schaeffler-model for the Schaeffler-bearings.

2.2.2 Clutch

In a dual clutch transmission (DCT), as the name suggests, there exists two different clutches for operating even and odd gears of the transmission separately. At any point during the operation when power is transferred, there will be one engaged clutch to facilitate the gear in use and one disengaged clutch, ready to switch to the next gear in line. The torque transfer in the engaged clutch happens

due to friction between a number of separate rotating discs connected to the engine and transmission input shaft respectively. For the disengaged clutch, the rotating discs are disconnected and separated by a small gap. As a result, there is no torque transfer through mechanical connection from the engine to the transmission. Both clutches can be disengaged if a gear is skipped so that the current gear and the next gear are on the same input shaft.
Due to high temperatures generated by the friction between the clutch discs, there is a necessity for cooling and lubricating these clutches to keep them from wearing out. For the engaged clutch, there is no interference from the lubricant to its operation. However, for the disengaged clutch, due to relative motion between the clutch discs, there is a viscous resistance to rotation due to the presence of the lubricant between the discs. This resistance generated is termed as clutch drag torque [14].

Several papers have been written trying estimate the drag torque originating from the clutches. The first model was developed by Kitabayashi et al. [19] which estimates the drag torque due to laminar flow of lubricant between the clutch disc gaps. However, the model does not consider the rupturing of oil film at high speeds and as a result produces unreliable results at higher speeds. Another model developed by Yuan et al. [40] is an improved version of the Kitabayashi model, which considers the resistance offered by the oil in the ruptured section while making contact with both the clutch discs. However, the model developed by Shoaib et al. [14] considers a more realistic and detailed approach towards estimating the drag torque from the clutch by considering a mist region and an oil region within the ruptured section of the oil film.

The same cylindrical co-ordinate system is used for all models:

- z, coincides with the rotating axis of the clutch
- θ, angular position around z
- r, radial distance from z

2.2.2.1 Model 1

The model developed by Shoaib et al. [14] is based on a simplification of continuity and Navier-Stokes equations. Assumptions are made before developing the model:

- The resistance to the flow of oil between the clutch discs results in shear forces for the discs and hence the flow is assumed to be viscous
- The flow is assumed to be laminar (Re<2000) which generally holds good for open wet clutches
- The lubricant flow geometry, feed rate and boundary conditions do not change with respect to time and as a result, the flow is assumed to be steady state
- The flow is axially symmetrical with respect to the z-axis
- Forces due to gravity are negligible
- The fluid physical properties, in general, are more dependant on temperature than pressure. But, due to minimal variations in temperature and pressure of the lubricant between the clutch discs, the fluid properties (ρ, ν) are assumed to be constant
- The fluid is incompressible
- Generally, the gap between the clutch discs is very small compared to the outer radius of the clutches ($h \ll R_o$). Hence, the lubricant flow velocity within the gap in the axial (z) direction is neglected

Boundary conditions are defined using no-slip conditions:

- The radial velocity boundary condition is defined such that there is no flow of lubricant radially at the surfaces of both the clutch discs:

$$u_R(R,\theta,0) = 0 \qquad u_R(R,\theta,h) = 0 \tag{27}$$

- The circumferential velocity is defined by the speeds of the discs:

$$u_\theta(R,\theta,0) = R\omega_1 \qquad u_\theta(R,\theta,h) = R\omega_2 \tag{28}$$

- The pressure of oil at the outer radius of clutch is assumed to be equal to the ambient pressure which is assumed to be zero:

$$P(R_o,\theta,z) = P_a = 0$$

The original Navier-Stokes equations and the continuity equation are presented in cylindrical coordinates since the clutch is rotational symmetric:

$$\rho\left(\frac{Du_R}{Dt} - \frac{u_\theta^2}{R}\right) = -\frac{\partial p}{\partial R} + f_r + \nu_{dyn}\left(\nabla^2 u_R - \frac{u_R}{R^2} - \frac{2}{R^2}\frac{\partial u_\theta}{\partial \theta}\right) \tag{29}$$

$$\rho\left(\frac{Du_\theta}{Dt} + \frac{u_\theta u_R}{R}\right) = -\frac{1}{R}\frac{\partial p}{\partial \theta} + f_\theta + \nu_{dyn}\left(\nabla^2 u_\theta - \frac{u_\theta}{R^2} + \frac{2}{R^2}\frac{\partial u_R}{\partial \theta}\right) \tag{30}$$

$$\rho\frac{Du_z}{Dt} = -\frac{\partial p}{\partial z} + f_z + \nu_{dyn}\nabla^2 u_z \tag{31}$$

$$\frac{1}{R}\frac{\partial}{\partial R}(Ru_R) + \frac{1}{R}\frac{\partial}{\partial \theta}(u_\theta) + \frac{\partial u_z}{\partial z} = 0 \tag{32}$$

where

$$\frac{D}{Dt} = \frac{\partial}{\partial t} + u_R\frac{\partial}{\partial R} + \frac{u_\theta}{R}\frac{\partial}{\partial \theta} + u_z\frac{\partial}{\partial z} \tag{33}$$

$$\nabla^2 = \frac{\partial^2}{\partial R^2} + \frac{1}{R}\frac{\partial}{\partial R} + \frac{1}{R^2}\frac{\partial^2}{\partial \theta^2} + \frac{\partial^2}{\partial z^2} \tag{34}$$

where f is body forces. The assumptions and boundary conditions mentioned above allows for simplification of equations. A truncation is also made in order to simplify further. See details in Appendix A. Finally, the equations are:

$$\frac{\partial u_R}{\partial R} + \frac{u_R}{R} = 0 \tag{35}$$

$$-\frac{u_\theta^2}{R} = -\frac{1}{\rho}\frac{\partial p}{\partial r} + \frac{\nu_{dyn}}{\rho}\frac{\partial^2 u_R}{\partial z^2} \tag{36}$$

$$0 = \frac{\mu}{\rho}\frac{\partial^2 u_\theta}{\partial z^2} \tag{37}$$

$$0 = -\frac{\partial p}{\partial z} \tag{38}$$

Solving these equations (see Appendix A) yields the flow through the clutch:

$$Q_a = \underbrace{-\frac{\pi R h^3}{6\nu_{dyn}}\frac{dp}{dR}}_{\text{Poiseuille flow}} + \underbrace{\frac{\rho\pi R^2 h^3}{6\nu_{dyn}}\left(\omega_1^2 + \omega_1\Delta\omega + \frac{3}{10}\Delta\omega^2\right)}_{\text{Centrifugal flow}} \tag{39}$$

At low rotational speeds the Poiseuille flow, or pressure induced flow, dominates the equation. As the rotational speed increases, so does the centrifugal force [1] and the flow generated by it. Since the actual flow, Q_a, is constant, the Poiseuille flow must reduce until its limitation at zero. According to Kato et al. [18] and Yuan et al. [38], this causes cavitation and there is no longer full film lubrication in the clutch. According to Yuan et al. [39] and Yuan et al. [40], there is a ruptured region spreading from the outside inwards with rivulets of lubricant film and mist in between, see figure 7. According to Reynold's cavitation boundary condition:

$$\frac{dp}{dR} = 0 \tag{40}$$

where the cavitation starts. This reduces equation 39 to:

$$Q_a = \frac{\rho\pi R_*^2 h^3}{6\nu_{dyn}} \left(\omega_1^2 + \omega_1\Delta\omega + \frac{3}{10}\Delta\omega^2\right) \tag{41}$$

where R_* is the effective radius up to which there exists full film lubrication. Outside this radius, there is a ruptured film consisting of a combination of partly oil/air mist and partly an oil film, see figure 7. The area ratio between the mist and film in the ruptured region is denoted ϕ. This ratio is calculated as the ratio between actual flow and needed flow to keep full film. The mist's region contribution to the flow is assumed to be negligible.

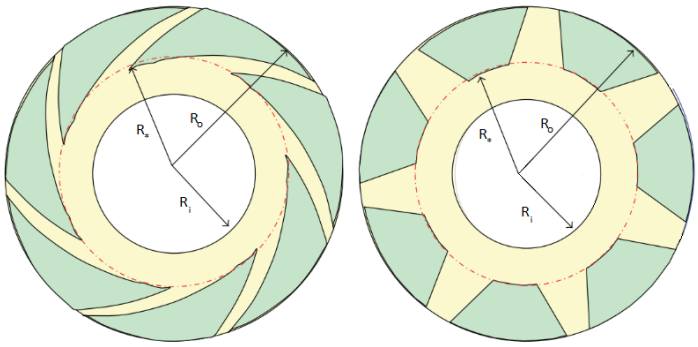

Figure 7: Full film region and ruptured region with combined film and mist, [14]

The left part of figure 7 shows a realistic view of the oil film where there is a full film to a certain radius which is then ruptured into mist (green) and rivulets of oil. The right part shows a simplification of the rivulets for easier calculations.

$$Q_a = \phi 2\pi R \int_0^h u_R dz = \phi Q_c \tag{42}$$

$$\phi = \frac{Q_a}{Q_c} = \frac{6\nu_{dyn} Q_a}{\rho\pi R^2 h^3} \left(\frac{1}{\omega_1^2 + \omega_1\Delta\omega + \frac{3}{10}\Delta\omega^2}\right) \tag{43}$$

With shear stress calculated according to the Newtonian frictional theorem:

$$\tau_{z\theta} = \nu_{dyn}\frac{\partial u_\theta}{\partial z} = \nu_{dyn}\frac{\partial\left(R\left(\omega_2 - \omega_1\right)\frac{z}{h} + \omega_1\right)}{\partial z} = \frac{\nu_{dyn} R\Delta\omega}{h} \tag{44}$$

The drag torque contribution from each region can be calculated by integrating the shear and leverage arm over the clutch discs:

[1] The authors of this thesis note that the "centrifugal force" does not exist strictly physically speaking. However, it is possible to calculate it and use it in engineering applications.

- Full film region:

$$T_{ff} = \int_0^{2\pi} \int_{R_i}^{R_*} n_i R \tau_{z\theta} R dR d\theta = \frac{\pi \nu_{dyn} \Delta\omega n_i}{2h} (R_*^4 - R_i^4) \tag{45}$$

- Ruptured film region:

$$T_{rf} = \int_0^{2\pi} \int_{R_*}^{R_o} n_i \phi r \tau_{z\theta} R dR d\theta = \frac{6\nu_{dyn}^2 \Delta\omega Q_a n_i}{\rho h^4} \frac{1}{\omega_1 + \omega_1 \Delta\omega + \frac{3}{10}\Delta\omega^2} \left(R_o^2 - R_*^2\right) \tag{46}$$

- Mist region:

$$\begin{aligned} T_{mf} &= \int_0^{2\pi} \int_{R_*}^{R_o} n_i (1-\phi) R \tau_{z\theta} R dR d\theta \\ &= \frac{2\pi \nu_{dyn,mist} \Delta\omega n_i}{h} \left(\frac{1}{4} \left(R_o^4 - R_*^4\right) - \frac{6\nu_{dyn} Q_a}{\rho \pi h^3} \frac{1}{\omega_1 + \omega_1 \Delta\omega + \frac{3}{10}\Delta\omega^2} \left(R_o^2 - R_*^2\right) \right) \end{aligned} \tag{47}$$

where n_i is the amount of frictional interfaces. According to Shoaib et al. [15], when the flow is constant, the viscosity of the mist is around 1/900th of that of the lubricant. To account for the effect of grooves on the friction disc, an area ratio is applied:

$$T_{clutch} = \gamma (T_{ff} + T_{rp} + T_{mf}) \tag{48}$$

where γ:

$$\gamma = \frac{A_{ng}}{A_{tot}} \tag{49}$$

2.2.2.2 Model 2

Li et al. [13] developed a mathematical model to provide a method for determining the shrinking oil film radius between the clutch discs and finally estimate the clutch drag torque. Before developing the mathematical model, a certain number of assumptions were made:

- Oil flow is in-compressible and steady state
- Oil flow is laminar and symmetrical
- Gravitational effects can be neglected
- The clutch discs are assumed to have no grooves
- The two clutch discs on a friction pair have no sliding effect on the oil layer above them

Once the assumptions were made, the boundary conditions for the fluid flow are defined:

- Radial velocity boundary conditions:

$$u_R(R, \theta, 0) = 0 \qquad u_R(R, \theta, h_i) = 0 \tag{50}$$

- Circumferential velocity boundary conditions:

$$u_\theta(R, \theta, 0) = 0 \qquad u_\theta(R, \theta, h_i) = R\Delta\omega \tag{51}$$

As can be seen in equation 51, this model only considers the relative speed between the discs and not their respective absolute speed, i.e. the slowest disc is considered stationary. The flow equations are defined using the continuity and Navier-Stokes equations in cylindrical coordinate system given by equations 29-34. Simplifying these equations based on the assumptions and the boundary conditions yield (see Appendix B):

$$-\frac{\partial p}{\partial R}+\nu_{dyn}\frac{\partial^2 u_R}{\partial z^2}=\rho\left(u_R\frac{\partial u_R}{\partial R}-\frac{u_\theta^2}{R}\right) \tag{52}$$

$$\nu_{dyn}\frac{\partial^2 u_\theta}{\partial z^2}=\rho\left(u_R\frac{\partial u_\theta}{\partial R}+\frac{u_\theta u_R}{R}\right) \tag{53}$$

$$\frac{\partial p}{\partial z}=0 \tag{54}$$

The oil pressure gradient across the radius of the oil film is then determined by making use of the boundary conditions and the simplified flow equations in equations 52-54:

$$\frac{\partial p}{\partial R}=\frac{27\rho Q^2}{70\pi^2 h_i R^3}+\frac{3\rho\Delta\omega^2 R}{10}-\frac{6\nu_{dyn}Q}{\pi R h_i^3} \tag{55}$$

Integrating the pressure gradient along the radial direction and considering the boundary condition yields the pressure distribution of the oil within the friction gap:

$$p(R)=-\frac{27\rho Q^2}{140\pi^2 h_i^2}R^{-2}+\frac{3}{20}\rho\omega^2 R^{-2}-\frac{6\nu_{dyn}Q}{\pi h_i^3}ln(R)+C \tag{56}$$

In an actual scenario, there always exists an oil pressure difference between the inlet and outlet of the friction pair and as a result the pressure difference is determined:

$$p(R_i)-p(R_o)=\Delta p \tag{57}$$

This pressure difference is however small according to Yuan et al. [40]. Substituting equation 56 into equation 57 and rearranging the terms will produce the equation to estimate the required flow rate of oil, Q_r, within the friction gap to maintain a full oil film:

$$Q_r=\frac{\frac{6\nu_{dyn}}{\pi h_i^3}ln\left(\frac{R_i}{R_o}\right)}{\frac{27\rho}{70\pi^2 h_i^2}\left(R_o^{-2}-R_i^{-2}\right)}+\frac{\sqrt{\left(\frac{6\nu_{dyn}}{\pi h_i^3}ln\left(\frac{R_i}{R_o}\right)\right)^2-\frac{81\rho^2\Delta\omega^2\left(R_o^{-2}-R_i^{-2}\right)\left(R_i^2-R_o^2\right)-540\rho\left(R_o^{-2}-R_i^{-2}\right)\Delta p}{700\pi^2 h_i^2}}}{\frac{27\rho}{70\pi^2 h_i^2}\left(R_o^{-2}-R_i^{-2}\right)} \tag{58}$$

It is evident from equation 58 that the required oil flow rate to keep the friction gap filled with oil is dependent on the relative speed difference between the clutch discs on either sides of the friction pair. The dependency of required oil flow rate on the relative speed is such that the required flow rate increases with increase in speed but the actual flow rate is a constant and, as a result, the oil film in the friction gap reduces in radial size as the speed goes up.
To determine the effective oil film radius i.e the shrink radius of the oil film at various speeds, the actual, Q_a, and required flow rates, Q_r, are compared:

- If $Q_a \geq Q_r$:

$$R_*=R_o \tag{59}$$

- If $Q_a < Q_r$, i.e when the actual amount of oil flowing through the friction gap is less than what is required to keep a complete oil film, the effective outer radius is determined based on the relationship between the oil flow rate and the volumes at inlet and outlet of the friction gap:

$$\frac{R_*^2\pi h-R_i^2\pi h}{Q_a}=\frac{R_o^2\pi h-R_i^2\pi h}{Q_r} \tag{60}$$

$$\implies R_* = \sqrt{\frac{Q_a}{Q_r}R_o^2 + R_i^2\left(1 - \frac{Q_a}{Q_r}\right)} \tag{61}$$

Finally, the drag torque arising from each of the friction gap is determined in analogy with 45:

$$T_{drag,clutch,i} = \frac{\pi \nu_{dyn} \Delta\omega}{2h_i}\left(R_*^4 - R_i^4\right) \tag{62}$$

The total drag torque due to the disengaged clutch is then determined by summing up the drag torque from all of the friction pairs, n_i:

$$T_{drag,clutch} = \sum_{i=1}^{N} T_{drag,clutch,i} \tag{63}$$

To account for grooves in friction discs, the same area method is used as described in equations 48 and 49.

2.2.2.3 Model 3

Yuan et al. [40] provides another model to calculate the drag torque in a wet clutch. The model is based on the simplified Navier-Stokes equations according to Hashimoto et al. [12]:

$$-\frac{\rho u_\theta^2}{R} = -\frac{\partial p}{\partial R} + \frac{\partial \tau_{rz}}{\partial z} \tag{64}$$

$$0 = -\frac{1}{R}\frac{\partial p}{\partial \theta} + \frac{\partial \tau_{\theta z}}{\partial z} \tag{65}$$

$$\frac{1}{R}\frac{\partial (R u_R)}{\partial R} + \frac{1}{R}\frac{\partial u_\theta}{\partial \theta} + \frac{\partial u_z}{\partial z} = 0 \tag{66}$$

According to Yuan et al. [40], clutches work at near-atmospheric pressure with little difference between inner and outer pressure. The oil is moved outward by a centrifugal force which is counteracted by viscous forces and surface tension. The importance of surface tension compared to viscous and hydrodynamic forces can be determined by the capillary number, Weber's number, Reynold's number and Bond's number. However, in a typical clutch the conditions are not satisfied in order to ignore surface tension.
No slip boundary conditions:

$$u_R(R,\theta,0) = 0 \qquad u_R(R,\theta,h) = 0 \tag{67}$$

$$u_\theta(R,\theta,0) = R\Delta\omega \qquad u_\theta(R,\theta,h) = 0 \tag{68}$$

Also, the clutch gap is small so there is no velocity along z. Integrating the governing equations 64, 65 and 66 along z from 0 to h:

$$-\frac{\rho}{R}\int_0^h u_R^2 dz = -\frac{\partial p}{\partial R}h + \tau_{rz}(h) - \tau_{rz}(0) \tag{69}$$

$$0 = \tau_{\theta z}(h) - \tau_{\theta z}(0), \left(\frac{\partial p}{\partial \theta} = 0, \text{ due to symmetric flow}\right) \tag{70}$$

$$\frac{\partial}{\partial R}\left(R\int_0^h u_R dz\right) + \frac{\partial}{\partial \theta}\left(\int_0^h u_\theta dz\right) = 0 \tag{71}$$

According to [40], following equations are approximations of shear stress terms:

$$\tau_{rz}(h) - \tau_{rz}(0) \approx -\frac{\nu_{dyn}}{hG_r} u_{rm} \tag{72}$$

where u_{rm} is the mean radial velocity.

$$\tau_{\theta z}(h) - \tau_{\theta z}(0) \approx -\frac{\nu_{dyn}}{hG_\theta} \left(u_{\theta m} - \frac{R\Delta\omega}{2} \right) \tag{73}$$

where $u_{\theta m}$ is the mean circumferential velocity.

$$\int_0^h u_\theta^2 dz \approx h u_{\theta m}^2 + f r^2 \Delta\omega^2 h \tag{74}$$

where the average speeds can be calculated according to:

$$u_{im} = \frac{1}{h} \int_0^h u_i dz, \quad i = R, \theta \tag{75}$$

$$f = \begin{cases} 0,885 Re_h^{-0,367}, & Re_h \leq 500 \\ 0,09 & Re_h > 500 \end{cases} \tag{76}$$

where

$$Re_h = \frac{\rho \Delta\omega R h}{\nu_{dyn}} \tag{77}$$

and G_r and G_θ are turbulence coefficients according to:

$$G_r = \frac{1}{12} \left(1 + 0,00069 Re_h^{0,88} \right) \tag{78}$$

$$G_\theta = \frac{1}{12} \left(1 + 0,00069 Re_h^{0,95} \right) \tag{79}$$

Combining 69, 72 and 74:

$$\frac{\rho}{R} \int_0^h u_\theta^2 dz = \frac{\partial p}{\partial R} h + \frac{\nu_{dyn}}{hG_r} u_{rm} \tag{80}$$

$$\implies \frac{\rho}{R} \left(u_{\theta m}^2 h + f r^2 \omega^2 h \right) = \frac{\partial p}{\partial R} h + \frac{\nu_{dyn}}{hG_r} u_{rm} \tag{81}$$

$$\implies \frac{\rho}{R} u_{\theta m}^2 + f \rho R \Delta\omega^2 = \frac{\partial p}{\partial R} + \frac{\nu_{dyn}}{h^2 G_r} u_{rm} \tag{82}$$

Combining 70 and 73:

$$u_{\theta m} = \frac{R\Delta\omega}{2} \tag{83}$$

Combining 82 and 83 and rearranging:

$$\frac{\partial p}{\partial R} = -\frac{\nu_{dyn}}{h^2 G_r} u_{rm} + \rho R \Delta\omega^2 \left(f + \frac{1}{4} \right) \tag{84}$$

The radial flow through a cylinder can be calculated through:

$$Q = 2\pi R_m u_{rm} h \tag{85}$$

Inserted into 84, introducing an effective radius, $R_* < R_o$, for when the flow is less than required for a full film to form and calculating pressure difference between and arbitrary point and inlet:

$$p(R) - p(R_i) = -\frac{\mu Q}{2\pi R_m h^3 G_r} (R - R_i) + \frac{\rho \Delta\omega^2}{2} \left(f + \frac{1}{4} \right) \left(R^2 - R_i^2 \right) \tag{86}$$

Where the full film ends, a pressure jump occurs. The pressure difference between the two sides of the surface is related to the curvature:

$$\underbrace{p\left(R_{*-}\right)}_{\text{pressure inside surface}} - \overbrace{p\left(R_{*+}\right)}^{pressureoutsidesurface} = \sigma\left(k_\theta + k_z\right) \tag{87}$$

where σ is the oil surface tension coefficient, k_θ is the circumferential curvature and k_z is the curvature along z, see figure 8. Since $k_\theta << k_z$ the pressure jump is approximated with:

$$p\left(R_{*-}\right) - p\left(R_{*+}\right) = \frac{\sigma}{R} = \frac{2\sigma\cos\left(\theta\right)}{h} \tag{88}$$

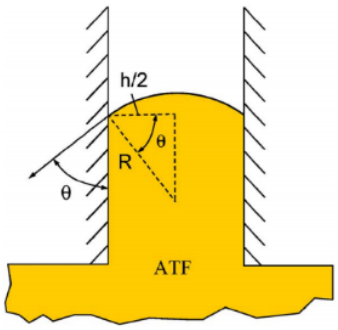

Figure 8: Surface shape at border between film and air, [40]

With the assumption that the pressure difference is small, 86 now becomes:

$$0 = -\frac{\nu_{dyn}Q}{2\pi R_m h^3 G_r}\left(R - R_i\right) + \frac{\rho\Delta\omega^2}{2}\left(f + \frac{1}{4}\right)\left(R^2 - R_i^2\right) - p\left(R_{*-}\right) - p\left(R_{*+}\right) = \frac{\sigma}{R} = \frac{2\sigma\cos\left(\theta\right)}{h} \tag{89}$$

According to Hashimoto et al. [12], the shear tension between plates can be calculated according to:

$$\tau_{\theta z} = \frac{\nu_{dyn}\Delta\omega R}{h}\left(1 + 0,0012Re_h^{0,94}\right) \tag{90}$$

Integrating for total drag torque:

$$T_{drag,clutch} = 2\pi n_i \int_{R_i}^{R_*} \frac{\nu_{dyn}\Delta\omega R^3}{h}\left(1 + 0,0012Re_h^{0,94}\right) dR \tag{91}$$

To account for grooves in friction discs, the same area method is used as described in equations 48 and 49.

2.2.2.4 Model 4

Since models one and two for drag torque in the clutch are similar with only small differences in how they are derived, a hybrid model is created. One difference is in the simplification of the Navier-Stokes equations. While model one relies on truncation to simplify the equations, the second model keeps as all terms resulting in different flow rate equations. Another is in the way the drag torque from different regions are calculated. Model one identifies three regions; the full film region, the ruptured

region with film and the ruptured region with mist. Model two only identifies the full film region. Model four combines the different models by taking the flow equations from model two and the drag torque equations from model one. I.e., the required flow is calculated according to 58 while the drag torque is calculated according to 45, 46, 47 and 48.

2.2.2.5 Model 5

Another difference in how the Navier-Stokes equations are calculated between model one and two are the circumferential boundary conditions 28 and 51. Model one considers the rotational speed for both discs while model two only considers the relative speed between them. Model five is according to model four but with boundary conditions from model one. This alters the pressure derivative slightly:

$$\frac{\partial p}{\partial R} = \frac{27\rho Q^2}{70\pi^2 h_i R^3} + \rho R\left(\omega_1^2 + \omega_1\Delta\omega + \frac{3}{10}\Delta\omega^2\right) - \frac{6\mu Q}{\pi R h_i^3} \tag{92}$$

which yields the flow equation:

$$\begin{aligned} Q_r = & \frac{\frac{6\nu_{dyn}}{\pi h_i^3} ln\left(\frac{R_i}{R_o}\right)}{\frac{27\rho}{70\pi^2 h_i^2}\left(R_o^{-2} - R_i^{-2}\right)} \\ & + \frac{\sqrt{\left(\frac{6\nu_{dyn}}{\pi h_i^3} ln\left(\frac{R_i}{R_o}\right)\right)^2 - \frac{81\rho^2\left(\frac{10}{3}\omega_1^2 + \frac{10}{3}\omega_1\Delta\omega + \Delta\omega^2\right)\left(R_o^{-2} - R_i^{-2}\right)\left(R_i^2 - R_o^2\right) - 540\rho\left(R_o^{-2} - R_i^{-2}\right)\Delta p}{700\pi^2 h_i^2}}}{\frac{27\rho}{70\pi^2 h_i^2}\left(R_o^{-2} - R_i^{-2}\right)} \end{aligned} \tag{93}$$

The drag torque is then calculated according to 45, 46, 47 and 48.

2.2.3 Churning

According to Seetharaman and Kahraman [31], churning drag is a type of speed-dependent drag torque originating due to presence of lubricant/oil around the object in consideration. In this case, when a gear is dipped in oil, the gear rotates through the oil bath which offers resistance to the rotation from the teeth cavity region and gear side faces.

2.2.3.1 Model 1

A simple model for estimating the churning drag torque has been developed by the International Organization for Standardization [10] considering several parameters in order to develop accurate estimation of the churning drag torque for helical and spur gears.

The ISO model [10] introduces a gear dip coefficient term, indicating the amount the gear is dipped in oil. The convention behind using the dip coefficient is that a dip coefficient of f_g=1 indicates that the entire gear is submerged in oil while f_g=0 indicates that the gear is not dipped in oil at all. The dip coefficient is a function of speed meaning that at low speeds, the oil level with respect to the gear can be higher while at higher speeds, the oil level may reduce and thereby indicating lower coefficient values.

The churning loss is divided into three separate categories as mentioned below and then summed up to obtain the total churning loss for a particular gear dipped in a specific level of oil:

- Smooth outside diameter: This type is used when the component has a smooth outer diameter like that of a shaft

$$P_{SOD} = \frac{7.37 f_g \nu_{kin} n^3 d_{o,s}^{4.7} l_s}{A_g 10^{26}} \tag{94}$$

- Sides of the gear: This type is used to determine the viscous resistance that originates from both the gear sides

$$P_{side} = \frac{1.474 f_g \nu_{kin} n^3 d_o^{5.7}}{A_g 10^{26}} \tag{95}$$

- Teeth surfaces: This type of loss is used to determine the resistance that originates from the gear teeth

$$P_{tooth} = \frac{7.37 f_g \nu_{kin} n^3 d_o^{4.7} b \frac{R_f}{\sqrt{tan\beta}}}{A_g 10^{26}} \tag{96}$$

where A_g is an arrangement constant with a value of 0.2 and R_f is a roughness factor determined by an empirical relation according to:

$$R_f = 7.93 - \frac{4.648}{m_t} \tag{97}$$

The total churning power loss from each gear is obtained by summing up the individual losses given by equation 98:

$$P_{drag,churning,i} = P_{SOD,i} + P_{side,i} + P_{tooth,i} \tag{98}$$

The power loss from each gear is then converted to drag torque loss by using the equation 99:

$$T_{drag,churning,i} = \frac{P_{drag,churning,i} * 1000}{\omega_{gear,i}} \tag{99}$$

Finally, the drag torque due to churning from all the gears dipped in oil is obtained by summing up the individual gear churning drag torque, given by equation 100:

$$T_{drag,churn} = \sum_{i=1}^{n} T_{drag,churning,i} \tag{100}$$

2.2.3.2 Model 2

Changenet and Velex [5] proposed a new model along with experiments and a dimensional analysis. The model was developed for spur gears. They assumed the following variables to influence the drag torque from churning:

- Gear geometry characterized by:
  - Module
  - Pitch diameter
  - Face width
- Characteristics of the lubricant:
  - Viscosity
  - Density
  - Immersion depth
  - Volume of the oil reserve
- Dynamic parameters characterized by:
  - Gravitational acceleration

– Rotational speed

Now the drag torque from churning can be expressed as:

$$T_{drag,churn} = f(m, d_p, b, \nu_{dyn}, \rho, h_{imm}, V_0, g, \omega) \tag{101}$$

Changenet and Velex use the normalization of Boness' [3] which takes the form:

$$T_{drag,churn} = \frac{1}{2}\rho\omega^2 r_p^3 S_m C_m \tag{102}$$

where S_m is the surface area between the fluid and the gear and C_m is the dimensionless drag torque. The surface area is approximated by:

$$S_m = r_p^2(2\theta - \sin(2\theta)) + d_p b\theta + \frac{2z\theta h_{tooth} b}{\pi \cos\alpha} \tag{103}$$

where the first term is for the lateral surfaces and the last two terms are for the teeth. θ is the angle between a vertical line through the pinion center and a line through the contact point between the fluid and the pinion periphery and the pinion center (see figure 9).

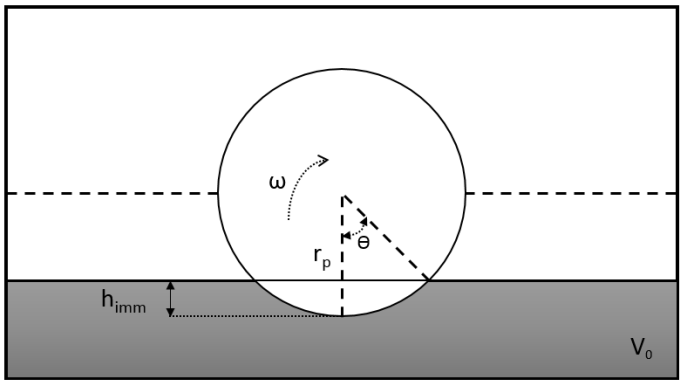

Figure 9: Churning of a gear

The dimensionless torque is expressed with seven groups of dimensionless quantities:

$$C_m = \psi_1 \left(\frac{m}{d_p}\right)^{\psi_2} \left(\frac{b}{d_p}\right)^{\psi_3} \left(\frac{h_{imm}}{d_p}\right)^{\psi_4} \left(\frac{V_0}{d_p^3}\right)^{\psi_5} Re^{\psi_6} Fr^{\psi_7} \tag{104}$$

Changenet and Velex use the pitch radius to define the Reynold's and Froude's numbers:

$$Re = \frac{\omega r_p^2}{\nu_{kin}} \tag{105}$$

$$Fr = \frac{\omega^2 r_p}{g} \tag{106}$$

According to Changenet and Velex [5], it was found that module has no effect on churning, so that $\psi_2 = 0$, and that there was no solution valid for all speeds. Instead, different coefficients are used at different speeds with linear interpolation in between. This speed is defined by a critical Reynold's number:

$$Re_c = \frac{\omega r_p b}{\nu_{kin}} \tag{107}$$

where a critical Reynold's number bellow 6000 is considered low speed and above 9000 is considered high speed.

Table 1: Coefficients for dimensional analysis

	ψ_1	ψ_2	ψ_3	ψ_4	ψ_5	ψ_6	ψ_7
Low-speed	$1,366$	0	0	$0,45$	$0,1$	$-0,21$	$-0,6$
High-speed	$3,644$	0	$0,85$	$0,1$	$-0,35$	0	$-0,88$

The losses from all gears are then summed up according to equation 100.

2.2.3.3 Model 3

Seetharaman and Kahraman [31] propose a model derived from Navier-Stokes equations. The model simplifies the gears as smooth cylinders. Therefore, no characteristics of the gear teeth are considered at all in the initial model. However, the model claims that with increased tooth height, the outer radius of the gear will increase which is considered in the model. The model identifies that at low rotational speed, great changes in tooth thickness will affect the model compared to the smooth cylinder assumption. The model uses Navier-Stokes equations which are simplified through the assumptions of:

- Steady state flow of oil around the gear
- Oil pressure only varies in radial direction
- Radial flow velocity of oil is zero
- Fluid is incompressible
- Oil density and viscosity are not affected by pressure
- Oil level within the transmission is considered static.
- The effect of flanges or casings are neglected
- The model considers only friction drag torque and not form drag torque

According to Johnston [16], form drag is the type of fluid resistance acting on an object based on its shape when a fluid flows towards it and friction drag is a type of fluid resistance due to the surface of the object as the fluid flows along the surface of the object.
The model identifies two different places where churning losses occur: along the the gear periphery and on the gear sides.

2.2.3.3.1 Periphery

For the periphery, the Navier-Stokes become after simplifications, in cylindrical coordinates:

$$\frac{\partial u_\theta}{\partial \theta} = 0 \tag{108}$$

$$\frac{\rho}{r} u_\theta^2 = \frac{\partial p}{\partial r} \tag{109}$$

$$\frac{\partial^2 u_\theta}{\partial r^2} + \frac{1}{r}\frac{\partial u_\theta}{\partial r} - \frac{u_\theta}{r^2} = 0 \tag{110}$$

With the boundary condition according to no slip at cylinder surface and no speed at infinite distance:

$$u_\theta(r_o) = \omega r_o \tag{111}$$

$$u_\theta(\infty) = 0 \tag{112}$$

Solving 110 and applying boundary conditions yields the tangential velocity along the periphery:

$$u_\theta = \frac{\omega r_o^2}{r}, \quad r \geq r_o \tag{113}$$

The shear stress components are calculated through:

$$\tau_{rr} = 2\nu_{dyn}\frac{\partial u_r}{\partial r} = 0 \tag{114}$$

$$\tau_{\theta\theta} = 2\nu_{dyn}\left(\frac{1}{r}\frac{\partial u_\theta}{\partial \theta} + \frac{u_r}{r}\right) = 0 \tag{115}$$

$$\tau_{r\theta} = \nu_{dyn}\left(r\frac{\partial}{\partial r}\left(\frac{u_\theta}{r}\right) + \frac{1}{r}\frac{\partial u_r}{\partial \theta}\right) = -\frac{2\nu_{dyn}\omega r_o^2}{r^2} \tag{116}$$

Now the tangential shear stress can be found at the periphery:

$$\tau_{r\theta}(r_o) = 2\nu_{dyn}\omega \tag{117}$$

So the drag force becomes:

$$F = A\tau_{r\theta} \tag{118}$$

where A is the wet area of the periphery:

$$A = 2r_o b cos^{-1}\left(1 - \frac{h_{imm}}{r_o}\right) \tag{119}$$

Therefore, if $\frac{h_{imm}}{r} \geq 2$ then $\frac{h_{imm}}{r} = 2$. This yields the force:

$$F = 4\nu_{dyn} b r_o \omega cos^{-1}\left(1 - \frac{h_{imm}}{r_o}\right) \tag{120}$$

Multiplying with the arm of leverage yields the drag torque:

$$T_{drag} = 4\nu_{dyn} b r_o^2 \omega cos^{-1}\left(1 - \frac{h_{imm}}{r_o}\right) \tag{121}$$

2.2.3.3.2 Sides

The model considers a laminar and a turbulent case for the sides of the gears which are simplified to flat discs. Reynold's number is defined as:

$$Re = \frac{2\rho\omega r^2}{\nu_{dyn}} \tag{122}$$

where a number below 10^5 is considered laminar and a number above 10^6 is considered turbulent. Linear interpolation is applied for the transitional region.
In the laminar region, the model assumes a linear velocity profile:

$$u_\theta = r_o\omega\frac{y}{\delta} \tag{123}$$

where y is the coordinate which the velocity profile varies along and δ is the boundary layer thickness, i.e. the distance from the surface until free stream velocity is essentially reached. The source defines the displacement thickness, i.e. the distance from the surface until free stream velocity is reached if friction doesn't exist with same flow loss as for the boundary layer, and the momentum thickness, i.e. same distance as displacement thickness but for equal momentum instead of flow according to Streeter and Wylie [33]:

$$\zeta = \int_0^\delta \left(1 - \frac{u_\theta}{r_o\omega}\right) dy = \frac{1}{2}\delta \tag{124}$$

$$\kappa = \int_0^\delta \frac{u_\theta}{r_o\omega}\left(1 - \frac{u_\theta}{r_o\omega}\right) dy = \frac{1}{6}\delta \tag{125}$$

where ζ is the distance the streamline is shifted from the surface of the gear and κ is the reduced momentum flux in the boundary layer due to shear stress (from friction) in contact with the gear.
A skin friction coefficient can be calculated through:

$$C = \frac{2\nu_{dyn}}{\rho r_o^2\omega^2}\frac{\partial u_\theta}{\partial y}\bigg|_{y=0} = \frac{2\nu_{kin}}{\delta r_o\omega} \tag{126}$$

The source uses the boundary layer integral equation of von Karman [17] to solve for boundary layer thickness, δ. The rate of increase in momentum thickness is directly proportional to the wall shear stress and therefore the coefficient of friction:

$$\frac{\partial\kappa}{\partial x} = \frac{1}{2}C \tag{127}$$

where x is a length parameter defined as $x = 2r_o\sin(1 - h_{imm}/r_o)$. Now, the boundary layer thickness can be solved for:

$$\delta = 3,46\sqrt{\frac{\nu_{kin}x}{r_o\omega}} \tag{128}$$

The boundary layer thickness can now be used to calculate the coefficient of friction:

$$C = 0,578\sqrt{\frac{\nu_{kin}}{xr_o\omega}} \tag{129}$$

Now, the frictional force on the sides of the disc can be calculated:

$$F = \frac{1}{2}\rho r_o^2\omega^2 AC \tag{130}$$

where A is the wet surface:

$$A = r_o^2\left(\frac{\pi}{2} - sin^{-1}\left(1 - \frac{h_{imm}}{r_o}\right) - \left(1 - \frac{h_{imm}}{r_o}\right)\sqrt{\frac{h_{imm}}{r_o}\left(2 - \frac{h_{imm}}{r_o}\right)}\right) \tag{131}$$

where if $h_{imm} \geq 2r_o$ the $h_{imm} = 2r_o$. Now the force can be calculated and multiplied with a factor 2 to consider both sides:

$$F = \frac{0,41\rho\nu_{kin}^{0,5}r_o^{1,5}\omega^{1,5}A}{\sqrt{r_o\sin\left(1 - \frac{h_{imm}}{r_o}\right)}} \tag{132}$$

which yields the drag torque:

$$T_{drag,churn} = \frac{0,41\rho\nu_{kin}^{0,5}r_o^{2}\omega^{1,5}A}{\sqrt{\sin\left(1 - \frac{h_{imm}}{r_o}\right)}} \tag{133}$$

For the turbulent case, the velocity follows the one seventh power law according to Streeter and Wylie [33]:

$$u_\theta = r_o\omega\left(\frac{y}{\delta}\right)^{\frac{1}{7}} \tag{134}$$

This alters the results for equations 124 and 125 for the streamline shift and momentum flux:

$$\zeta = \int_0^\delta \left(1 - \frac{u_\theta}{r_o\omega}\right) dy = \frac{1}{8}\delta \tag{135}$$

$$\kappa = \int_0^\delta \frac{u_\theta}{r_o\omega}\left(1 - \frac{u_\theta}{r_o\omega}\right) dy = \frac{7}{72}\delta \tag{136}$$

According to Streeter and Wylie [33], the coefficient of friction during turbulent flow is:

$$C = 0,02\left(\frac{\nu_{kin}}{r_o\omega\delta}\right)^{0,167} \tag{137}$$

In analogy with the laminar case, this yields the drag torque:

$$T_{drag,churn} = \frac{0,025\rho\nu_{kin}^{0,14}\omega^{1,86}r_o^{2,72}A}{\left(\sin\left(1 - \frac{h_{imm}}{r_o}\right)\right)^{0,14}} \tag{138}$$

The losses for all gears are then summed up according to 100.

2.2.4 Concentric Shaft Shear

A DCT, having two clutches to operate different sets of gears, contains two input shafts that are connected to the respective sets of gears. The input shafts in the DCT are arranged in such a way that one input shaft is a solid shaft passing concentrically through another input shaft which is hollow, while both the shafts are supported by bearings.
Due to the presence of bearings between the two shafts as support, lubrication is needed in between the shafts to keep the bearings from wearing out. As a result, there is lubricant flowing in the annular region between the two input shafts. This oil flow will tend to produce a viscous resistance onto the rotation of the input shafts.

Schlichting [30] proposed an equation to estimate the resisting torque originating onto the shafts due to the oil flow between the two concentric objects based on the Navier-Stokes equations. An assumption is made that the outer shaft is rotating while the inner shaft is made to stay still and thus the relative speed difference is equal to the speed of rotation of the outer shaft. The drag torque is given by:

$$T_{drag,shafts} = 4\pi\nu_{dyn}l_s\frac{r_{is,o}^2 r_{os,i}^2}{r_{os,i}^2 - r_{is,o}^2}\Delta\omega \tag{139}$$

where $r_{is,o}$ is the outer radius of the inner concentric shaft and $r_{os,i}$ is the inner radius of the outer concentric shaft.

2.2.5 Windage

Gears rotating in a transmission have resistance to rotation due to the presence of oil as stated in section 2.2.3. There also exists a resisting force to the rotation of all the gears within the transmission due to the presence of air and air-oil vapour inside the transmission and this resisting force leads to

windage loss. Dawson [7] derived empirical equations by allowing high-speed gears to slow down in absence of power.

Before carrying out the experiments, Dawson made some simplifications to his model:

- The gears in the experiment were surrounded by air only while in an actual scenario, there exists air-oil vapour as well
- The experiments were conducted on gears that were not meshed assuming that the mesh would not influence the windage losses in a significant way
- The experiments were mainly carried out on large spur gears and helical gears but the relation does not provide evaluation of the windage losses on helical gears

The empirical relation to calculate the windage power loss for a single gear contains the power loss at the tooth periphery and the gear sides separately and is given by:

$$P_{loss,windage} = n^{2.9} \left(\underbrace{0.16 d_r^{3.9}}_{\text{sides}} + \underbrace{d_r^{2.9} b^{0.75} m^{1.15}}_{\text{periphery}} \right) 10^{-20} \xi \lambda \tag{140}$$

where ξ is a constant dependent on the surrounding of the gear, such as flanges, shields or other gears, and λ is another constant dependent on the gearbox casing. According to Townsend [35] and Dawson [7], the casing has a great effect on windage losses. A tight fitting case around the gears can reduce the windage losses with between 50-60%.

The drag torque due to windage loss for a single gear is then determined from the basic power-torque relation:

$$T_{drag,windage,i} = \frac{P_{loss,windage,i} \cdot 1000}{\omega_i} \tag{141}$$

Finally, the drag torque from all the gears is summed up to obtain the total windage drag torque for the entire transmission:

$$T_{drag,windage} = \sum_{i=1}^{n} T_{drag,windage,i} \tag{142}$$

2.2.6 Pocketing

According to Concli and Gorla [6], there is a power loss due to a phenomena called pocketing (also called squeezing) in a gear mesh. This occurs when the volume between two faces reduces as gears are meshing. This causes an axial flow of the lubricant which introduces a loss for the system.

2.2.6.1 Maurer model

Franco and Carlo [6] provides a simple model first proposed by Maurer [22]. It is based on empirical observations.

$$T_{drag,pocketing} = 1,17 * 10^{-6} v_t^{1,95} i^{0,73} b^{1,37} \tag{143}$$

2.2.6.2 Mauz model

Franco and Carlo [6] also provides a model first proposed by Mauz [23]. It takes more factors into account such as fluid properties and gear pair setup and rotational direction. The source states that Mauz's model is the most complete one even though it is not very accurate and has limited range of application. Mauz's model varied the viscosity from 30 to 240 mm^2/s and states that the model has an uncertainty of 15% for results above 5 Nm and above 50% for results below 5 Nm. The model is for gears with a minimum 10° helix angle and a module of 4,5.

$$T_{drag,pocketing} = 0,0235\rho b r_p v_t^{1,2} C_s \tag{144}$$

where b is given in mm and C_s is a variable accounting for setup and rotational direction according to figure 10.

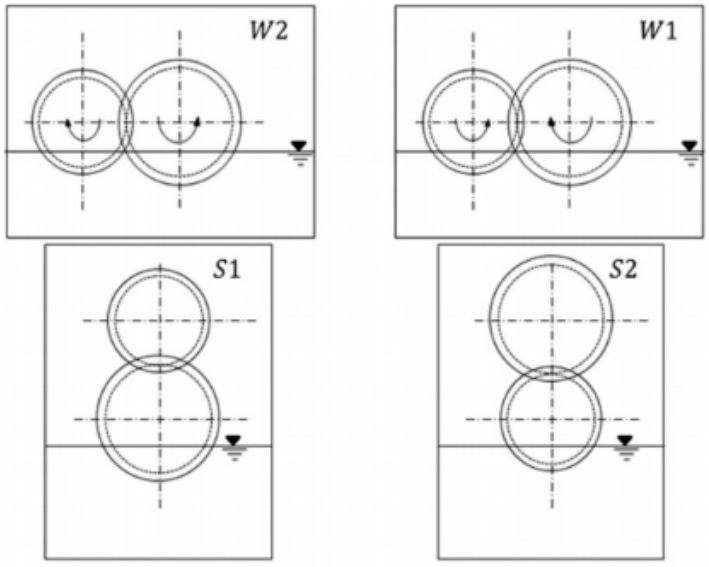

Figure 10: Different cases for pocketing, [6]

$$C_s = \frac{e}{h}, \quad for\ W_1 \tag{145}$$

$$C_s = 0, \quad for\ W_2 \tag{146}$$

$$C_s = \left(\frac{e}{h}\right)^2, \quad for\ S_1\ and\ S_2 \tag{147}$$

where e is the immersion depth and h is the pinion diameter.

2.2.7 Gear mesh

According to Seetharaman et al. [34], when a pinion and a gear are meshing under torque, a drag torque is generated. There is a load-dependent part and a speed-dependent part, described in 2.2.6. The load-dependent part is generated by the lubricated contacts and can loosely be seen as friction. These losses originate from relative speeds, both sliding and rolling, between the two contacting surfaces.

The sliding power loss at any instant is contributed by the gear mesh between the engaged gears and the gear mesh between the final drive gears. As a result, the total sliding loss is determined as the sum of the loss originating from the engaged gear and the final drive gears. Finally, the total power loss is divided by the engine speed to obtain the drag torque due to gear mesh, at the input shaft.

$$P_{loss,gear} = P_{loss,sliding,engagedgear} + P_{loss,sliding,finaldrive} \tag{148}$$

2.2.7.1 Model 1

According to Walker et al. [37], International Organization for Standardization [11] and Zhou et al. [41], the frictional torque from gear meshing can be calculated according to:

$$T_{drag,gear} = \frac{\mu T_{in} \cos^2(\beta)}{M} \tag{149}$$

where M is the mechanical advantage and is calculated through:

$$M = \frac{2\cos(\alpha)(H_s + H_t)}{H_s^2 + H_t^2} \tag{150}$$

where H_s and H_t are the sliding ratios at start of approach and end of recess respectively. The sliding ratios are calculated, according to Stephen [26], by:

$$H_s = (i+1)\left(\sqrt{\frac{r_{o2}^2}{r_{p2}^2} - \cos^2(\alpha)} - \sin(\alpha)\right) \tag{151}$$

$$H_t = \frac{i+1}{i}\left(\sqrt{\frac{r_{o1}^2}{r_{p1}^2} - \cos^2(\alpha)} - \sin(\alpha)\right) \tag{152}$$

For the coefficient of friction, Zhou et al. [41] provides the following equation:

$$\mu = \frac{\nu_{kin}^{k_1} K^{k_2}}{k_4 v_t^{k_3}} \tag{153}$$

where K is the load intensity, k_4 a coefficient and k_1,k_2 and k_3 are modifiers. The model has the following conditions:

$$2 \leq v_t \leq 25\text{m/s} \tag{154}$$

$$1,4 \leq K \leq 14\text{MPa} \tag{155}$$

For k_1, k_2, k_3 and k_4, following values are provided:

Table 2: Coefficient and modifiers for coefficient of friction

k_1	k_2	k_3	k_4
-0.223	-0,4	0,7	3,239

The load intensity is calculated through:

$$K = \frac{1000 T_{in}(z_1 + z_2)}{2 b z_2 r_{p1}^2} \tag{156}$$

2.2.7.2 Model 2

According to Fernandes et al. [9] and Machado [21], the frictional torque can be calculated according to:

$$T_{drag,gear} = T_{in}\mu H_v \tag{157}$$

where H_v is a loss factor:

$$H_v = \frac{\pi(i+1)}{z_1 i \cos(\beta)}(1 - \epsilon + \epsilon_1^2 + \epsilon_2^2) \tag{158}$$

The loss factor, however, is considered to be valid for spur gears mostly.

An empirical model is provided for calculating the coefficient of friction:

$$\mu = 0,048 \left(\frac{\frac{F_{bt}}{b}}{V_{\Sigma c}\rho_g} \right)^{0,2} \nu_{kin}^{-0,05} R_a^{0,25} X_L \tag{159}$$

where F_{bt} is a force dependent on the tangential force and pressure angle, $V_{\Sigma c}$ is the speed at the rolling point, ρ_g is the curvature at the rolling point dependent on the gear helix angle, R_a is the equivalent surface roughness of the pinion and gear. For the tangential force:

$$F_{bt} = \frac{F_t}{cos\alpha} \tag{160}$$

where, F_t is the tangential force on the gear in newtons. For the curvature:

$$\rho_g = \frac{\rho_c}{cos\beta} \tag{161}$$

$$R_a = \frac{R_{a1} + R_{a2}}{2} \tag{162}$$

Table 3: Lubrication factor

Mineral oil	Polyalfaolefins and esters	Polyglycols	Phosphoric esters	Traction fluids
1	0,8	$0,75\left(\frac{6}{V_{\Sigma c}}\right)^{0,2}$	1,3	1,5

According to Diez-Ibarbia, [8], the rolling speed and the addendum contact ratios can be calculated:

$$V_{\Sigma c} = 2v_t \sin(\alpha) \tag{163}$$

$$\epsilon_i = \frac{\sqrt{r_{o,i}^2 - (r_{p,i}\cos(\alpha))^2} - r_{p,i}\sin(\alpha)}{\pi m \cos(\alpha)},\ i = 1,2 \tag{164}$$

2.2.7.3 Model 3

Fernandes et al. [9] provides a second way to calculate the loss factor H_v which was originally described by Niemann [25].

$$H_v = \left(1 + \frac{z_2}{z_1}\right) \frac{\pi}{z_1} \frac{\epsilon_\alpha}{\cos(\beta)} \left(\frac{1}{\epsilon_\alpha} - 1 + \left(2k_0^2 - 2k_0 + 1\right)\epsilon_\alpha\right) \tag{165}$$

where k_0 is a coefficient defined by Niemann [36] and is given by:

$$k_0 = \frac{z_1}{2\pi\epsilon_\alpha \frac{z_2}{z_1}} \left(\sqrt{\left(\frac{r_{og}}{r_{og}}\right)^2 \frac{1}{\cos^2(\alpha)} - 1} - \tan(\alpha)\right) \tag{166}$$

2.2.7.4 Model 4

Carlos Fernandes et al. [9] provides a third way to calculate the loss factor H_v which was originally described by Buckingham [4].

$$H_v = \left(1 + \frac{z_2}{z_1}\right) \frac{\pi}{z_1} \frac{\epsilon_\alpha}{\cos(\beta)} (2k_0^2 - 2k_0 + 1) \tag{167}$$

where k_0 is according to 166.

2.2.7.5 Model 5

Anderson et al. [1] gives a detailed mathematical model to estimate the power losses due to gears meshing, based out of experiments conducted on spur gears. Heingartner et al. [24] utilizes the model from Anderson and modifies the same to estimate gear mesh power loss on helical gears.

According to Heingartner et al. [24], the sliding power loss is given by:

$$P_{loss,sliding} = F_s \cdot V_s \tag{168}$$

where, F_s is the sliding force in newtons.

The sliding force is the frictional force generated due to mechanical contact between the mating gears teeth and is given by:

$$F_s = \mu \cdot N \tag{169}$$

where N is the normal tooth contact load in newtons.

The coefficient of friction is calculated based on the gear parameters and property of oil present between the mating gears:

$$\mu = 0.0127 \cdot \log\left(\frac{C_1 N}{\nu_{dyn,amb} V_s V_r L_c}\right) \tag{170}$$

where C_1 is a constant, $\nu_{dyn,amb}$ is the ambient fluid dynamic viscosity at ambient temperature and L_c is the average length of contact between the mating gears

The gear mesh power loss is then converted to drag torque by dividing the power loss with the rotational speed of the input shaft:

$$T_{drag,gear} = \frac{P_{loss,gear}}{\omega_{engine}} \tag{171}$$

2.2.8 Relative speed

Since many of the sources of drag torque depend on the speed difference between the two input shafts, this has to be determined. With only one gear engaged and torques acting on it (i.e. the drag torque) are unknown, this has been determined through physical testing.

2.3 Synchronizer evaluation

In order to evaluate the synchronizer ring, all torques acting on need to be determined. Except for the drag torque modelled in previous sections, friction torque and indexing torque can be calculated [20]:

$$T_f = \frac{n_c \mu_{cones} d_{s,m} F_a}{2 \sin(\psi)} \tag{172}$$

$$T_z = F_a \frac{d_{s,p}}{2} \frac{\cos(\varphi) - \mu_d \sin(\varphi)}{\cos(\varphi) + \mu_d \sin(\varphi)} \tag{173}$$

When these two torques are known along with drag torque, the slip time it takes to synchronize can be calculated (assuming constant torques):

$$T = \frac{\Delta\omega}{\Delta t} J \tag{174}$$

$$\implies \Delta t = \frac{J}{T} \Delta\omega \tag{175}$$

where T is the sum of torques. It should be noted that the friction torque and the gearing torque are always oppositely directed while the drag torque is in the direction of the frictional torque at up-shifts and in the opposite direction at down-shifts. From this, several parameters related to the specification of the friction lining can be calculated in order to dimension synchronizers:

$$W = \frac{1}{2} \left(-J\Delta\omega^2 \pm T_{drag} \Delta\omega \Delta t \right) \tag{176}$$

$$q_A = \frac{W}{A_s} \tag{177}$$

$$P_m = \frac{W}{\Delta t} \tag{178}$$

$$P_{mA} = \frac{q_A}{\Delta t} \tag{179}$$

$$v_{s,max} = \Delta\omega \frac{d_{s,max}}{2} \tag{180}$$

$$F_n = \frac{T}{\mu_{cones} \frac{d_{s,m}}{2} n_c} \tag{181}$$

$$p_m = \frac{F_n}{n_c A_s} \tag{182}$$

$$P_{max} = p_m v_{s,max} \mu_{cones} \tag{183}$$

The performance and durability of the synchronizers are assessed based on these parameters and their behaviour with respect to the design and quality limits. The synchronizer model developed in this thesis determines these parameters of the synchronizers in multiple operating conditions and compares them with their respective specifications. The considered parameters that the model validates are:

- Design parameters
  - Specific frictional power
  - Specific frictional work
  - Slip speed
  - Contact pressure
- Quality parameter
  - Slip time

Each of the above design parameters have specified limits to how much the synchronizers are able to handle while keeping their performance. The quality parameter also has specified limits to make the car enjoyable to drive. The axial force applied by the gear actuator to move the synchronizer towards the gear has pre-defined boundary limits.

3 Results

All results are normalized due to a confidentiality requirement from CEVT. Each normalization has been done with respect to the maximum value within each subsection, i.e. each drag torque source has been normalized with respect to its respective maximum value and total drag torques have been normalized with respect to the maximum total drag torque values at that operating condition.

3.1 Drag torque

3.1.1 Bearings

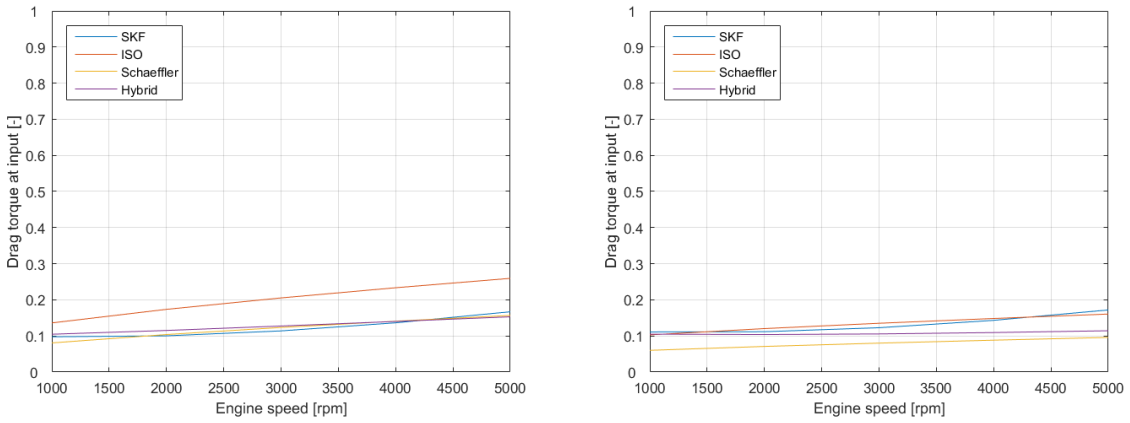

(a) 40°C **(b)** 80°C

Figure 11: Normalized drag torque for low gear at different temperatures and 50 Nm input torque

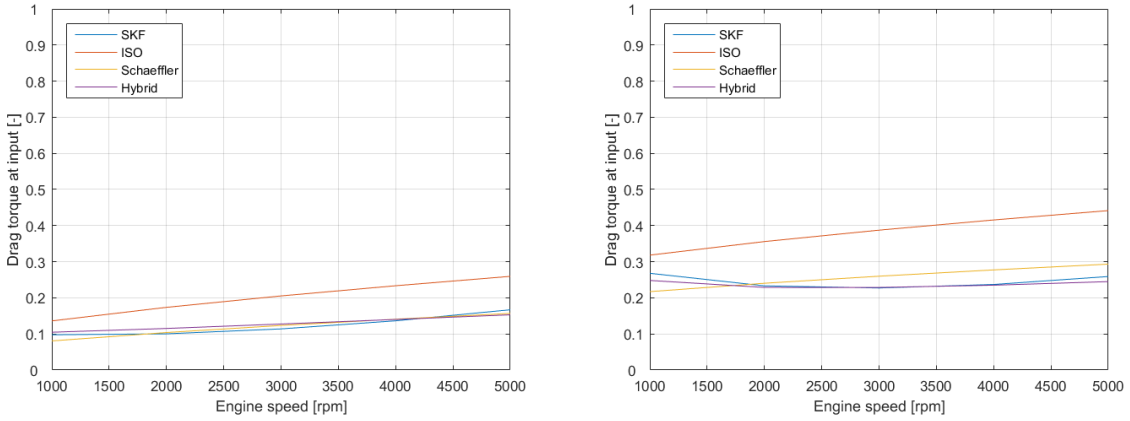

(a) 50 Nm **(b)** 150 Nm

Figure 12: Normalized drag torque for different input torques at low gear and 40°C

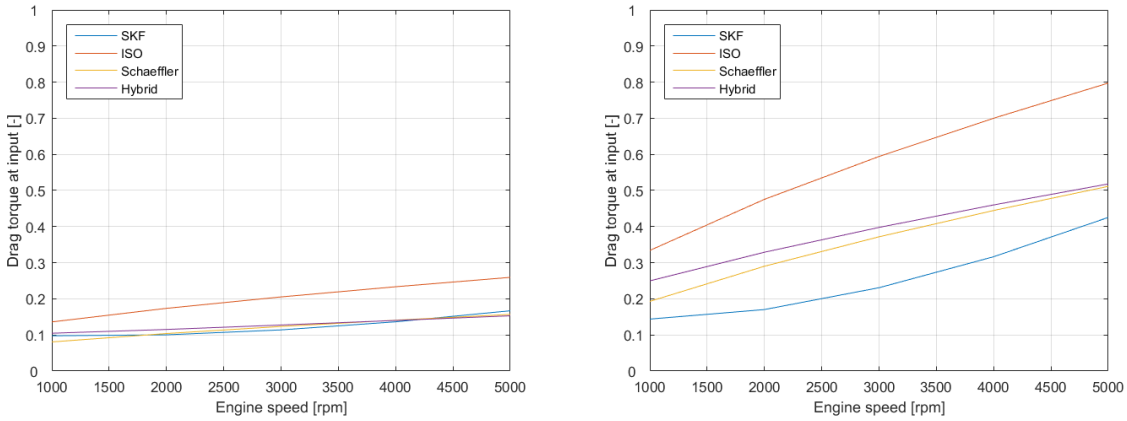

(a) Low gear **(b)** High gear

Figure 13: Normalized drag torque for different gears at 40°C and 50 Nm input torque

As seen in figure 11, an increased temperature decreases the drag torque from bearings in all models except the SKF model which even increases slightly. The decrease for the ISO and Schaeffler models is also bigger at higher speeds, resulting in a decrease in the gradient between drag torque and speed as well.
The same phenomena occurs at higher torques according to figure 12, but at a much greater magnitude for the SKF model. This also affects the hybrid model since it contains results from the SKF model.
In figure 13, it can be seen that at same operating conditions and different gears, the higher gear generates a significant increase in drag torque.
In figures 11 to 13, it is seen that at lower temperatures, the ISO model is considerably higher than the other models. At higher temperatures the SKF model closes in and in some cases becomes higher.
From figure 12, it can be seen that an increase of input torque with a factor of 3 yields a significant increase in drag torque.

3.1.2 Clutch

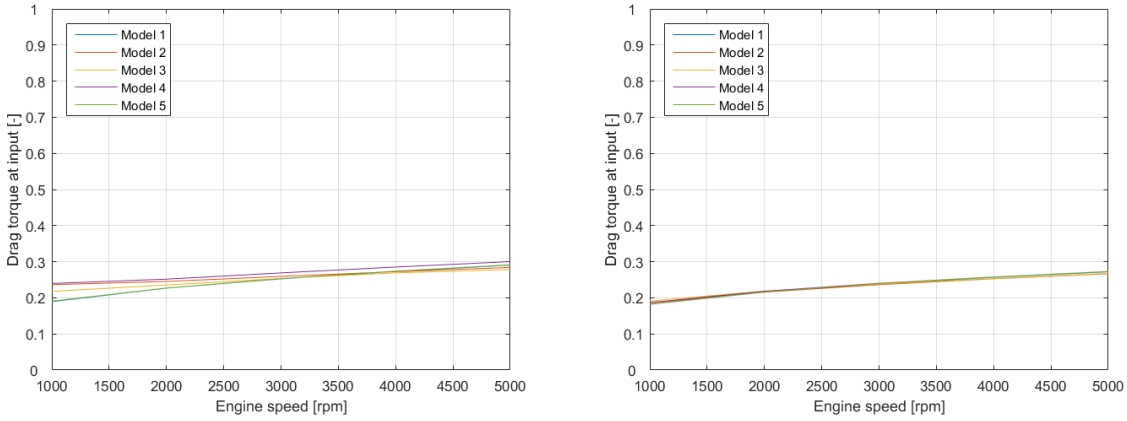

(a) $40°C$ **(b)** $80°C$

Figure 14: Normalized drag torque for low gear at different temperatures, small clutch gap and low oil flow

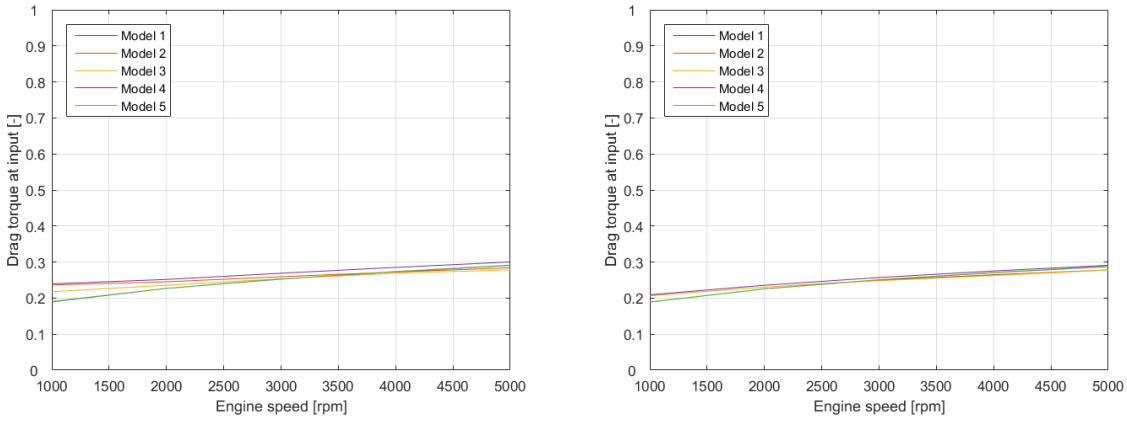

(a) Small gap **(b)** Big gap

Figure 15: Normalized drag torque for low gear with different clutch gaps, $40°C$ and low oil flow

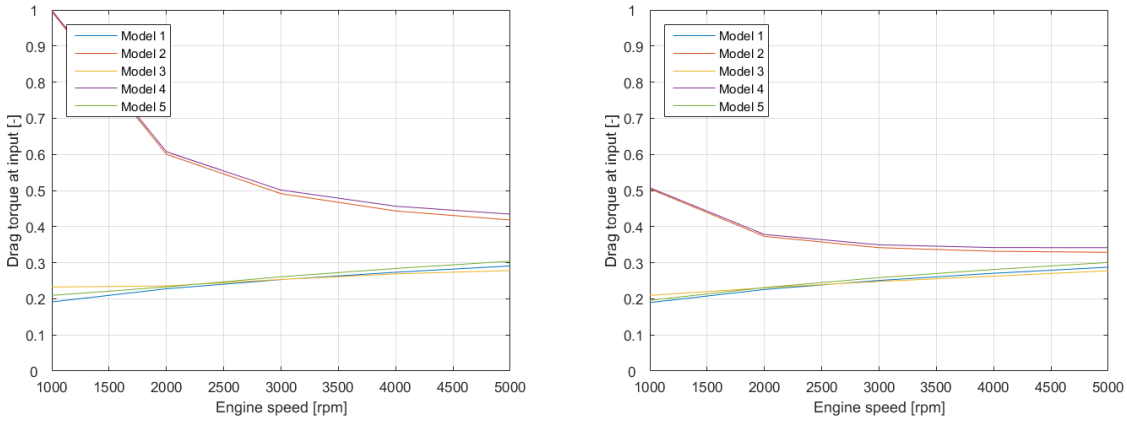

(a) Small gap **(b)** Big gap

Figure 16: Normalized drag torque for low gear with different clutch gaps, 40°C and high oil flow

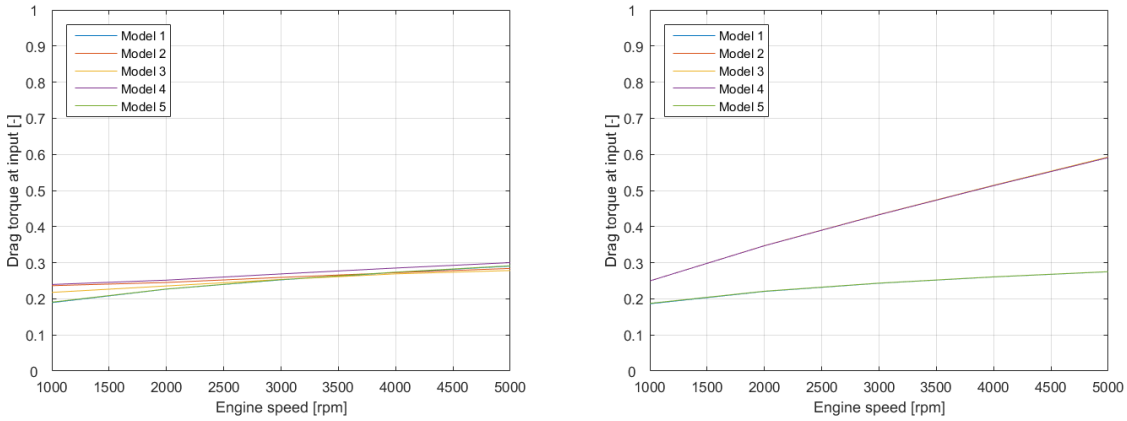

(a) Low gear **(b)** High gear

Figure 17: Normalized drag torque for different gears at 40°C, small clutch gap and low oil flow

In figure 17, model 1 coincides with model 5 in both figures, model 2 and 4 coincide in the right as well as model 3 and 5. From figure 14, it can be seen that temperature has a slight effect on clutch drag torque which is also different between the models. All results are decreasing with temperature and models appear close to one another at higher temperatures.
From figure 15, it can be seen that clutch gap has barely any effect on models 3, 4 and 5 while only slight differences appear for models 2 and 4 when the oil flow is low.
Between figures 15a and 16a, it can be seen that model 2 and 4 are greatly affected by increased oil flow, especially at lower speeds. The other models are also more affected at lower speeds than at higher speeds but with a smaller magnitude. From figure 16, it can also be seen that at a high oil flow, the effect of the clutch gap increases for model 2 and 4, especially at low speeds.
From figure 17, it can be seen that model 2 and 4 are greatly influenced by a higher gear at higher speeds while models 1, 3 and 5 are barely affected.

3.1.3 Churning

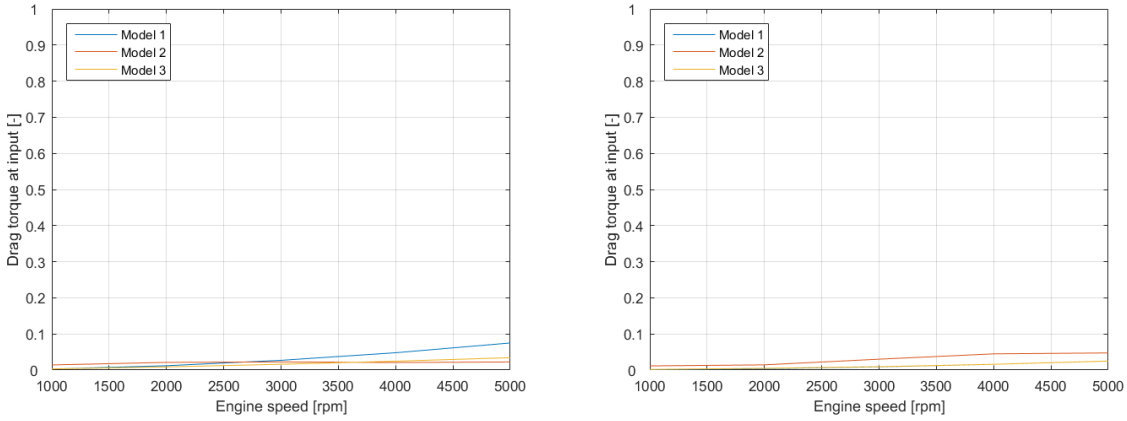

(a) 40°C **(b)** 80°C

Figure 18: Normalized drag torque for low gear with different temperatures and an small oil volume

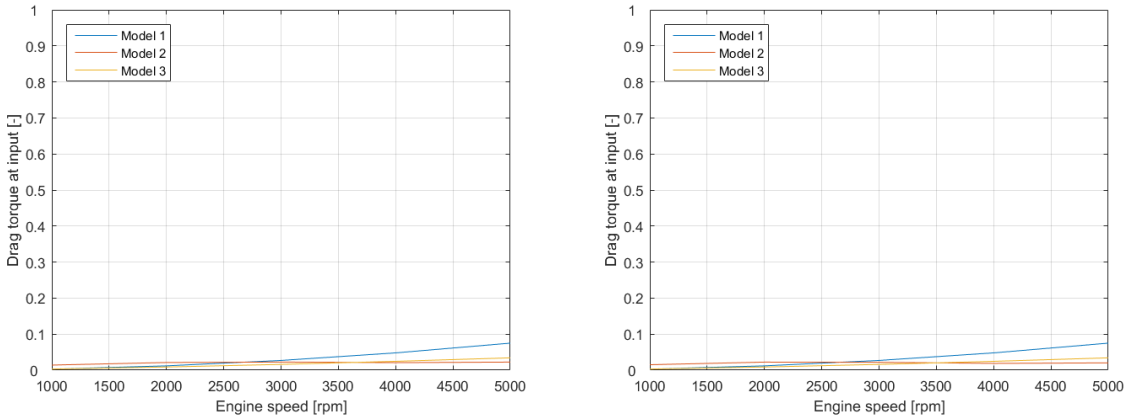

(a) Small volume **(b)** Big volume

Figure 19: Normalized drag torque for low gear at 40°C with different oil volumes

In figure 19 b, model 1 and 3 coincide.

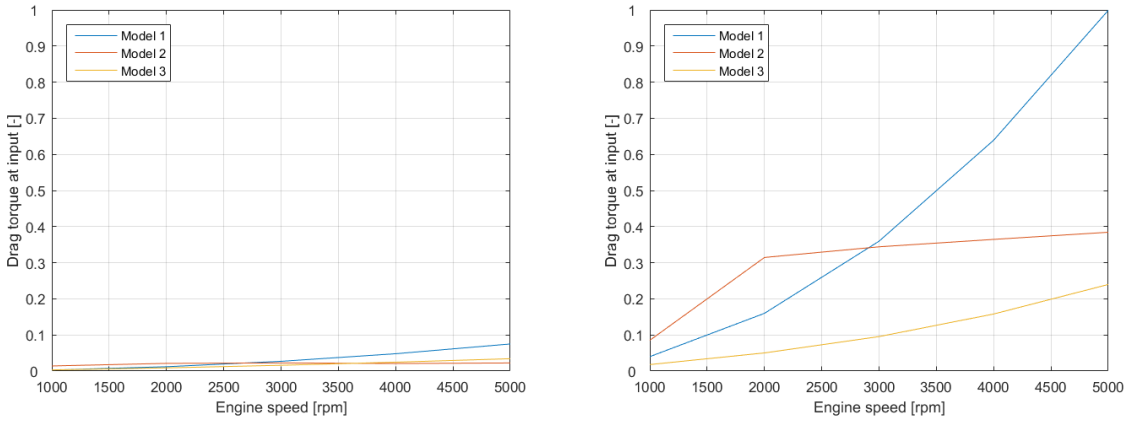

(a) Low gear **(b)** High gear

Figure 20: Normalized drag torque for different gears at $40°C$ and an small oil volume

From figure 18, it can be seen that temperature has a big effect on model 1, reducing it to virtually zero while model 2 is affected with a slight increase and model 3 is slightly reduced. The oil volume is only part of model 2 according to equation 104. However, in figure 19, it can be seen that this variable barely has any effect. From figure 20, it can be seen that a higher gear greatly increases drag torque for all models. Models 1 and 3 have gradients that increase with speed while the gradient for model 2 declines after 2000 revolutions per minute.

Table 4: Lowest and highest Reynold's number for oil flow around gears

Speed \ Temp	$40°C$	$80°C$
Low speed	630-3571	1907-10760
High speed	3164-17850	9533-53790

Based on model 2, table 4 gives the range of critical Reynold's number to depict the flow regimes of the oil around the gears at two different temperatures and speeds. A number bellow 6000 is considered laminar and a number above 9000 is considered turbulent, see equation 107. As seen from the table, the flow is laminar at lower temperatures except for a few gears at higher speed and tends to become turbulent at higher temperature.

3.1.4 Concentric shaft

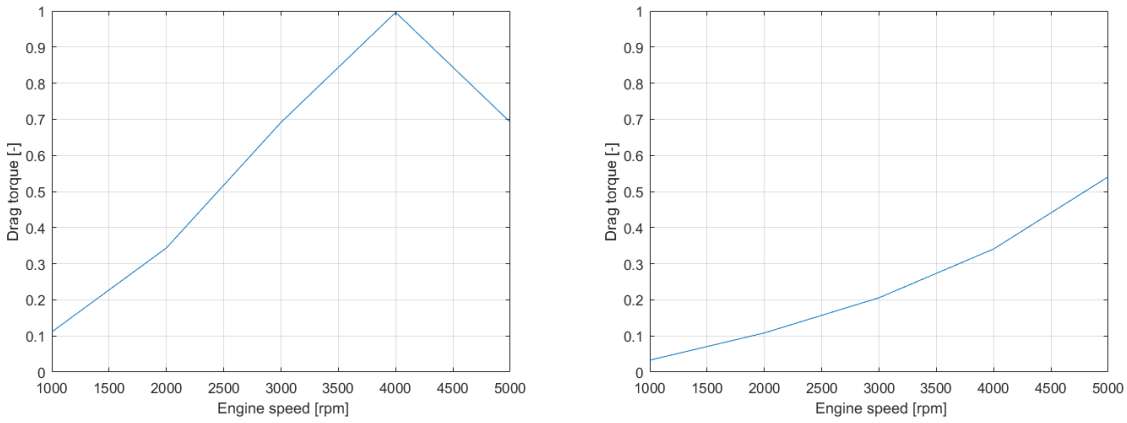

(a) 40°C **(b)** 80°C

Figure 21: Normalized drag torque for low gear at different temperatures

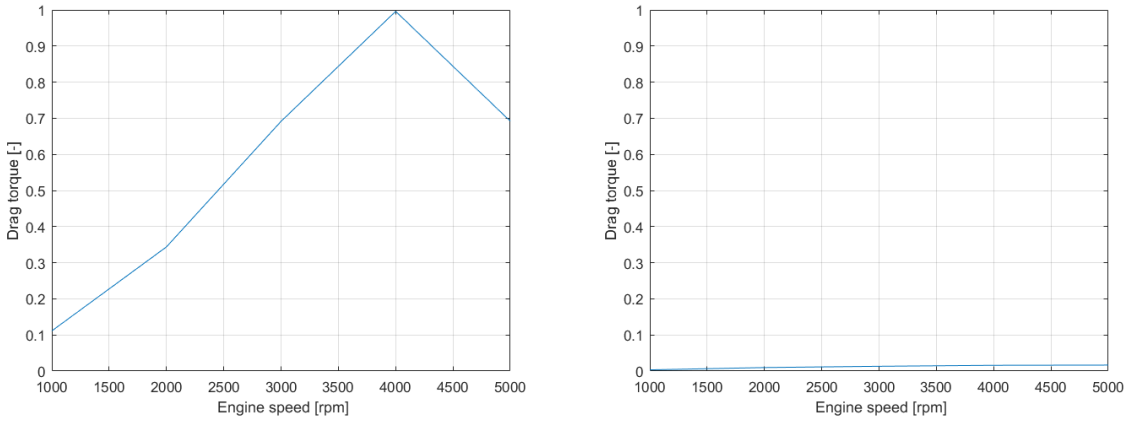

(a) Low gear **(b)** High gear

Figure 22: Normalized drag torque for different gears at 40°C

Figure 21 gives the comparison of concentric shaft drag torque for different temperatures when the same gear is engaged. It is evident that the drag torque reduces with increase in temperature. Figure 22 gives the comparison of concentric shaft drag torque for different gears when operated at the same temperature and is clear that the drag torque reduces at higher gears.

3.1.5 Windage

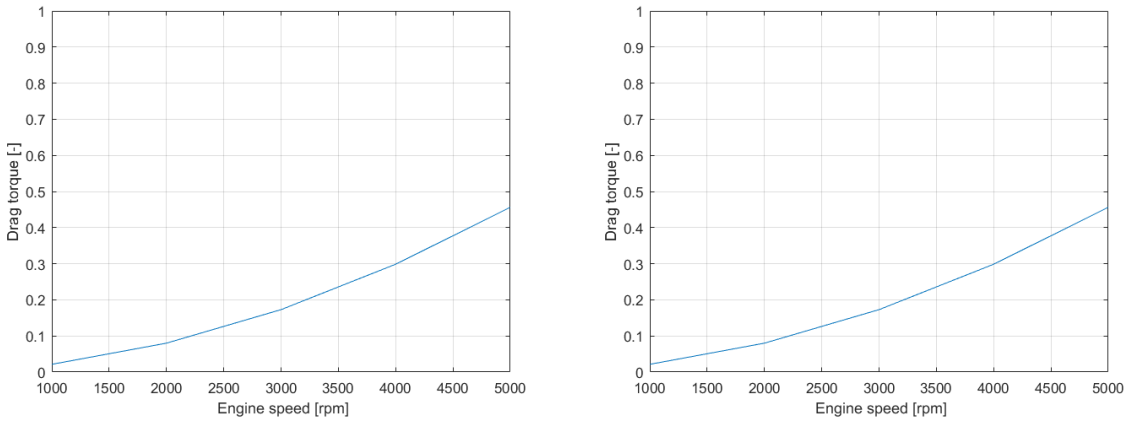

(a) 40°C **(b)** 80°C

Figure 23: Normalized drag torque for low gear at different temperatures

Figure 23 shows the effect of temperature on the windage drag torque when the transmission is run on same gear. It is seen that the windage drag torque is unaffected by change in temperature.

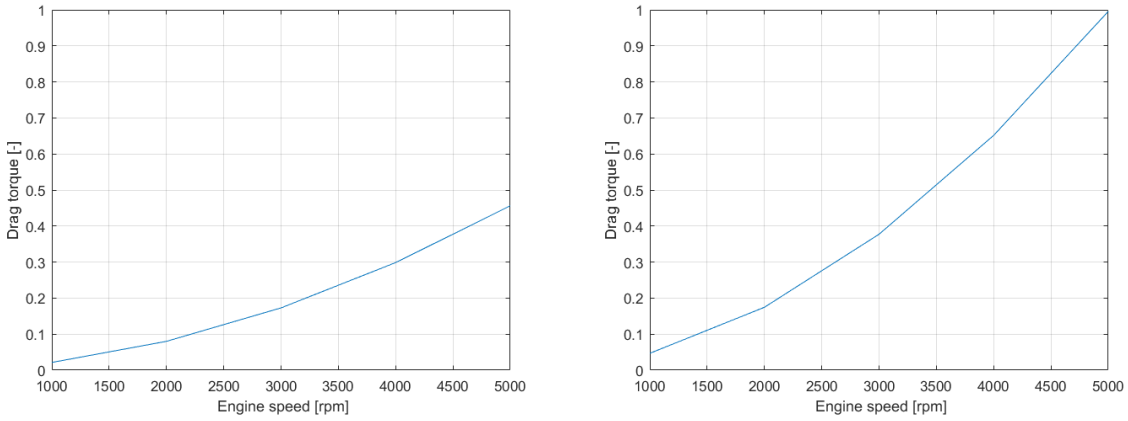

(a) Low gear **(b)** High gear

Figure 24: Normalized drag torque for different gears at 40°C

Figure 24 represents the comparison of windage drag torque when different gears are engaged at the same temperature. As seen in the figure, the windage drag torque increases with higher gears.

3.1.6 Pocketing

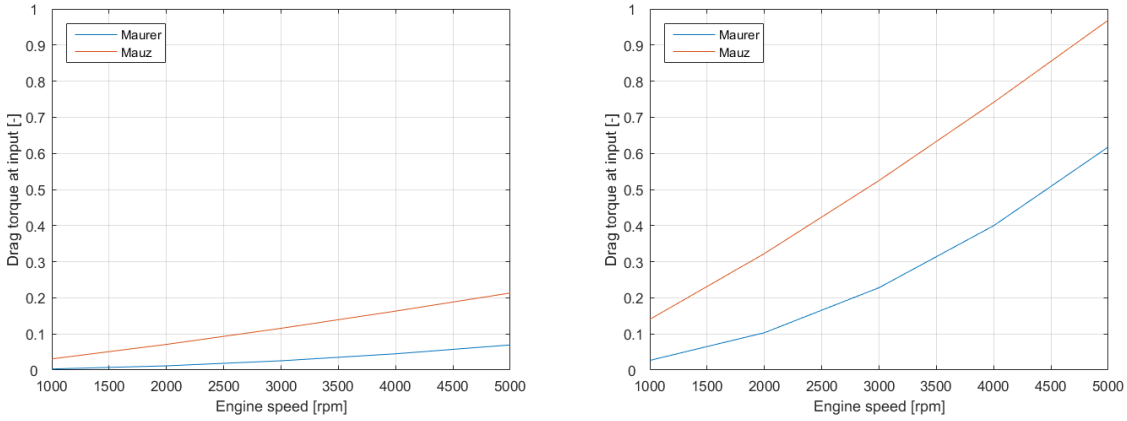

(a) Low gear **(b)** High gear

Figure 25: Normalized drag torque for different gears at $40°C$

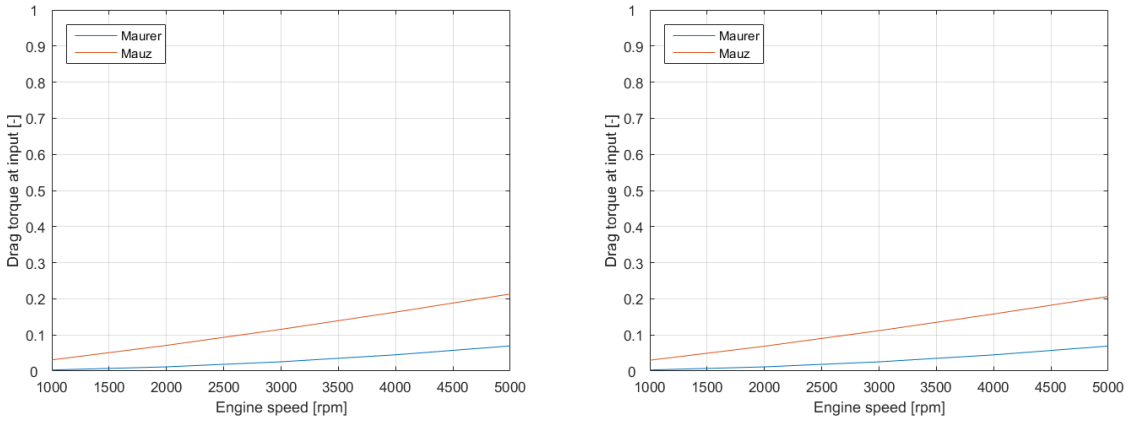

(a) $40°C$ **(b)** $80°C$

Figure 26: Normalized drag torque for low gear at different temperatures

From figure 25, it can be seen that a higher gear increases pocketing drag torque significantly. The increase is higher at higher speeds for Maurer's model than for Mauz's model, closing the gap between the models slightly. It can also be seen from figure 26 that temperature has only a slight effect, most visible at high speeds for Maurer's model.

3.1.7 Gear mesh

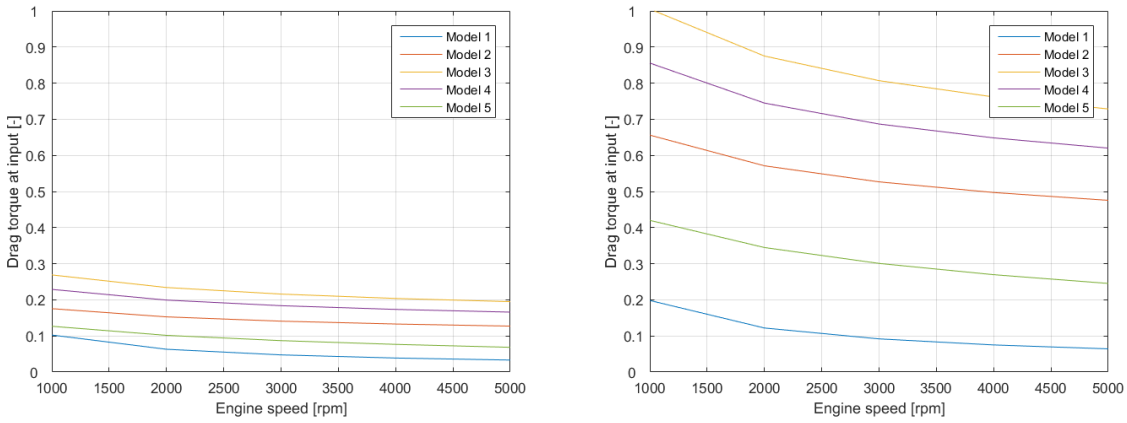

(a) 50Nm **(b)** 150Nm

Figure 27: Normalized drag torque for low gear at 40°C and different input torques

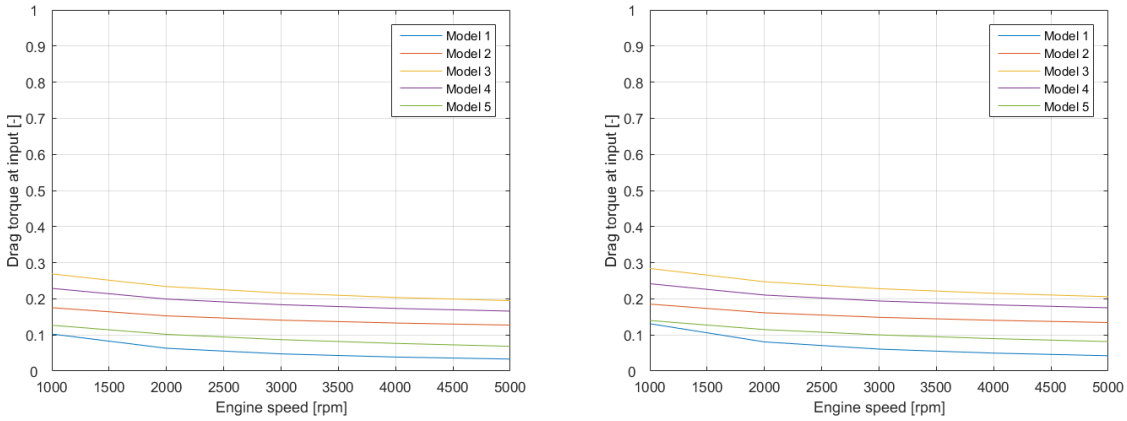

(a) 40°C **(b)** 80°C

Figure 28: Normalized drag torque for low gear at 50Nm input torque and different temperatures

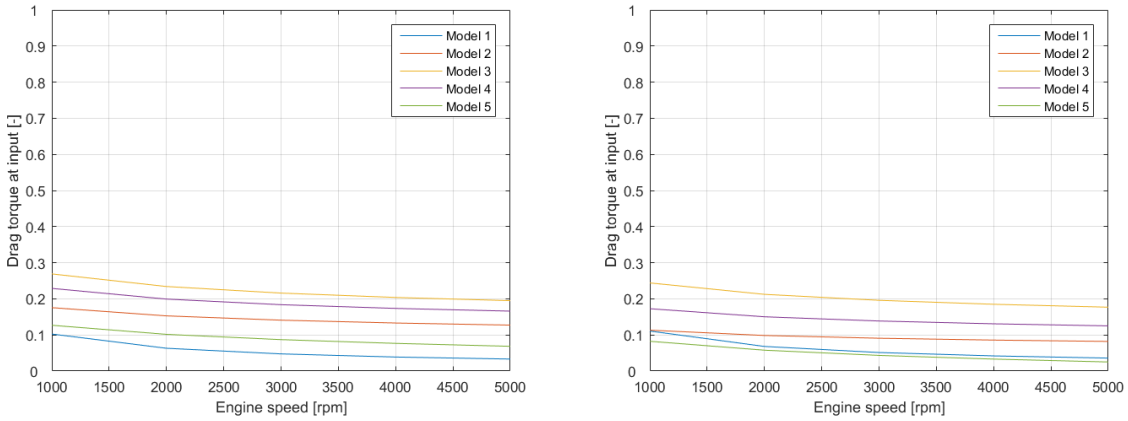

(a) Low gear **(b)** High gear

Figure 29: Normalized drag torque for different gears at 150Nm input torque and 40°C

Figures 27 to 29 show all the same tendency for how the drag torque behaves at various conditions between the models. However, they show very different absolute values among them.
Figure 27 shows that an increase in input torque results in an increase in frictional torque in the gear mesh. However, while the increase is around double for model 1, it is almost quadruple for model 3. The other models are almost consistently in between, regardless of operating conditions. Only when in a high gear is model 5 slightly lower than model 1.
Figure 28 shows an increase in drag torque when there is an increase in temperature. This change is much smaller than for the increase in input torque and seem to affect model 1 more than model 3 in contradiction to an increase in input torque.
Figure 29 shows a decrease in drag torque when a higher gear is engaged for model 2, 3, 4, and 5 and an slight increase for model 1.
Two things should be noted as for these results. Model 1 has conditions regarding load intensity and velocity according to equations 154 and 155. These condition were mostly fulfilled except at some very high loads combined with low gear and low speed or high gear and high speed. The other is that model 2, 3 and 4 contain a lubrication factor that was unknown for the used oil. For these results, X_L was set to 1. All three models scale linearly with this factor according to equation 159.

3.1.8 Relative speed

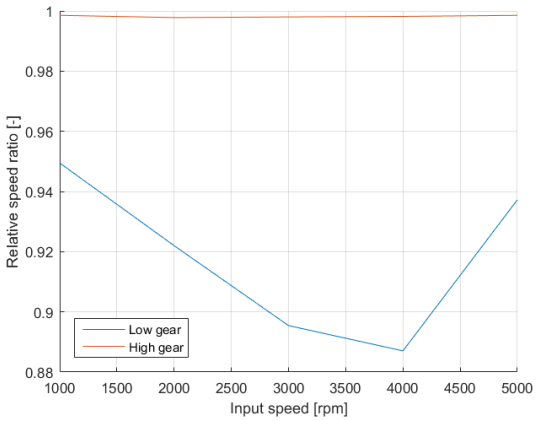

Figure 30: Relative speed between input shafts at different gears at $40°C$

As seen in figure 30, there is a significant difference in relative speed between the input shafts depending if a high or low gear is engaged. A lower gear is also more dependent on input speed than a higher gear.

3.1.9 Speed dependent

To model the drag torque for the complete gearbox, one model has to be selected for each source. This is explained in the discussion, see section 4. The speed-dependent model consists of following sub-models for each source of drag torque:

Table 5: Models for speed-dependent drag torque

Clutch	Pocketing	Churning
5	Mauz	2

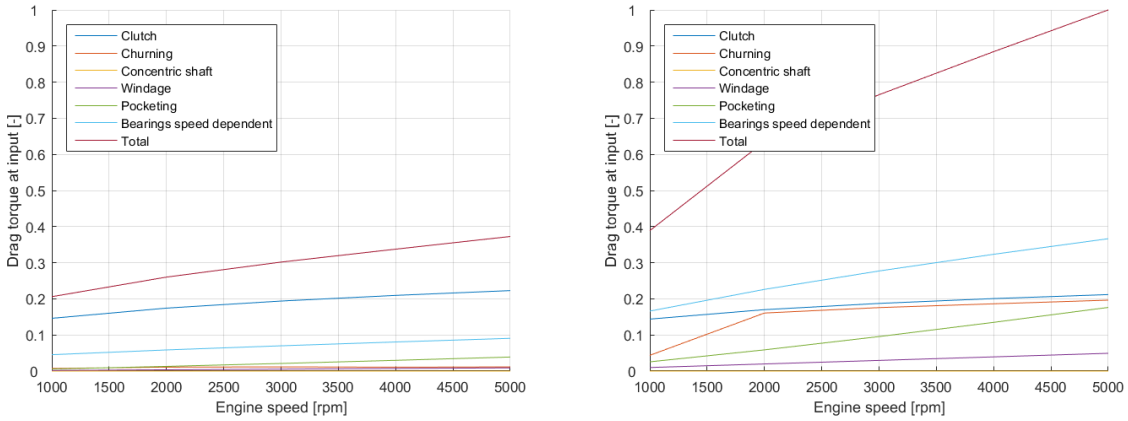

(a) Low gear **(b)** High gear

Figure 31: Normalized speed dependent drag torque in different gears at 40°C

It can be seen in figure 31 that a higher gear greatly increases speed dependent drag torque. The clutch is not much affected while churning and bearing speed dependent drag torque increase greatly. The total result doubles at low speeds and increases even more at high speeds.

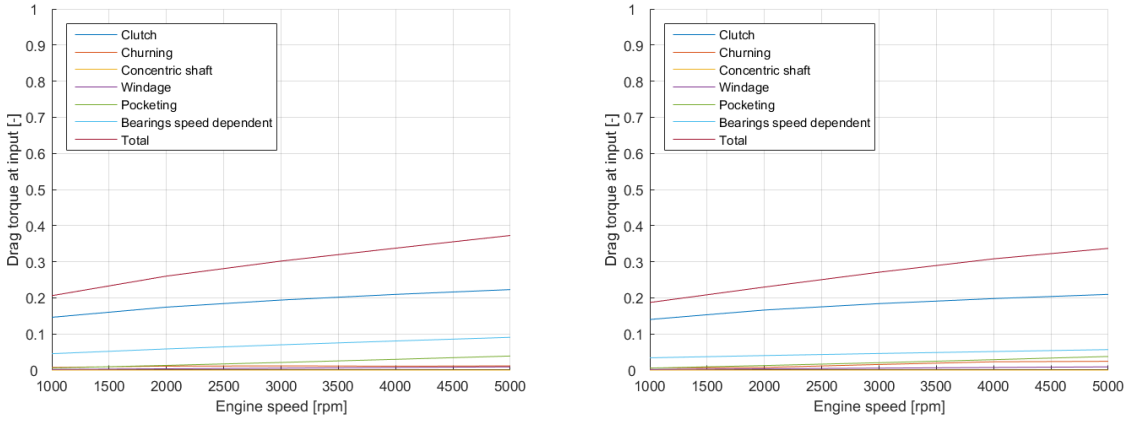

(a) 40°C **(b)** 80°C

Figure 32: Normalized speed dependent drag torque in different temperatures, low gear

From figure 32, it can be seen that temperature has a smaller effect than engaged gear on speed dependent drag torque. The total speed dependent drag torque decreases slightly at a higher temperature. Figure 33 shows how the dynamic oil viscosity varies with temperature. It can be seen that gradient becomes smaller and smaller and virtually tends towards zero after 40°C. However, the viscosity at 80°C is less than 35% of that at 40°C.

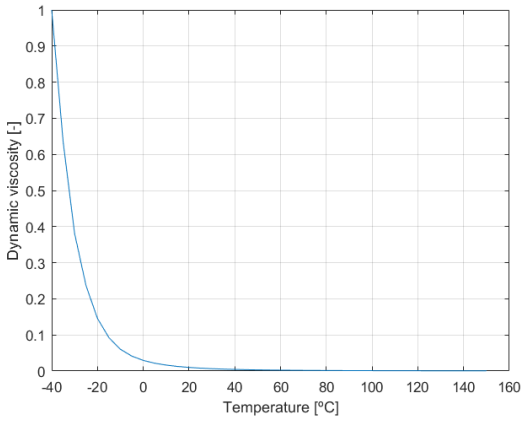

Figure 33: Dynamic viscosity of oil

3.1.10 Load dependent

To model the drag torque for the complete gearbox, one model has to be selected for each source. This is explained in the discussion, see section 4. The load-dependent model consists of following sub-models for each source of drag torque:

Table 6: Models for load-dependent drag torque

Bearings	Gear mesh
Hybrid	2

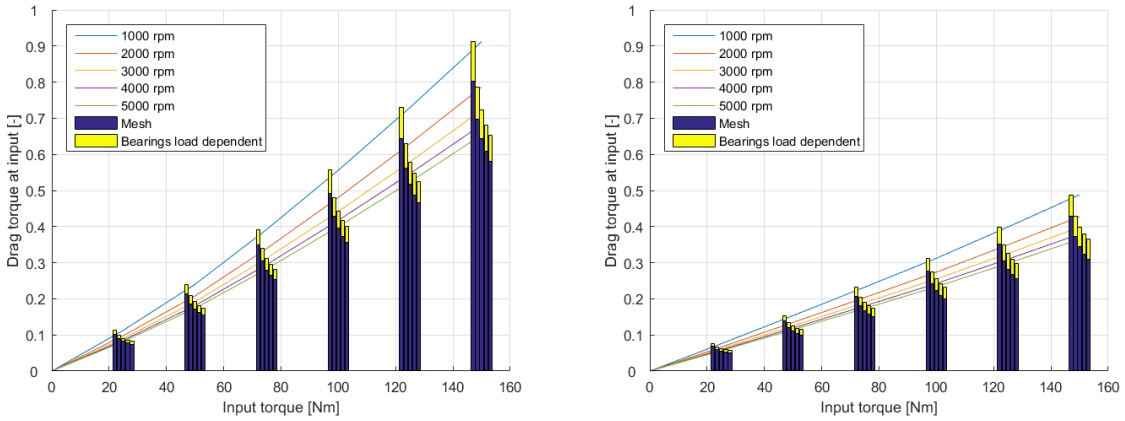

(a) Low gear **(b)** High gear

Figure 34: Normalized load dependent drag torque in different gears at $40°C$

From figure 34, it can be seen that the drag torque in the complete gearbox increases with increased input torque. Lower speeds also results in a higher load dependent drag torque, suggesting that there is some speed dependency in the load-dependent drag torque. Furthermore, it can be seen that the gear

mesh makes up for most of the load-dependent drag torque. The dependency between input torque and drag torque is almost linear.
Figure 34 also shows a decrease in drag torque at higher gears. A change from low gear to high gear almost halves the drag torque at otherwise same operating conditions.

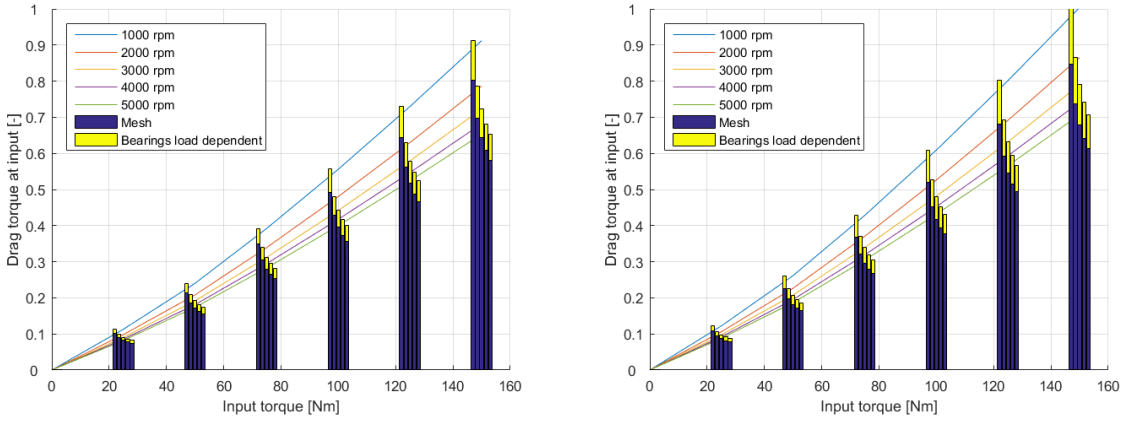

(a) $40°C$ **(b)** $80°C$

Figure 35: Normalized load dependent drag torque in different temperatures, low gear

From figure 35 it can be seen that temperature has an effect on load-dependent drag torque which produces higher drag torque at higher temperatures. The effect seems to be bigger on bearing load-dependent drag torque than on gear mesh drag torque.

3.1.11 Total

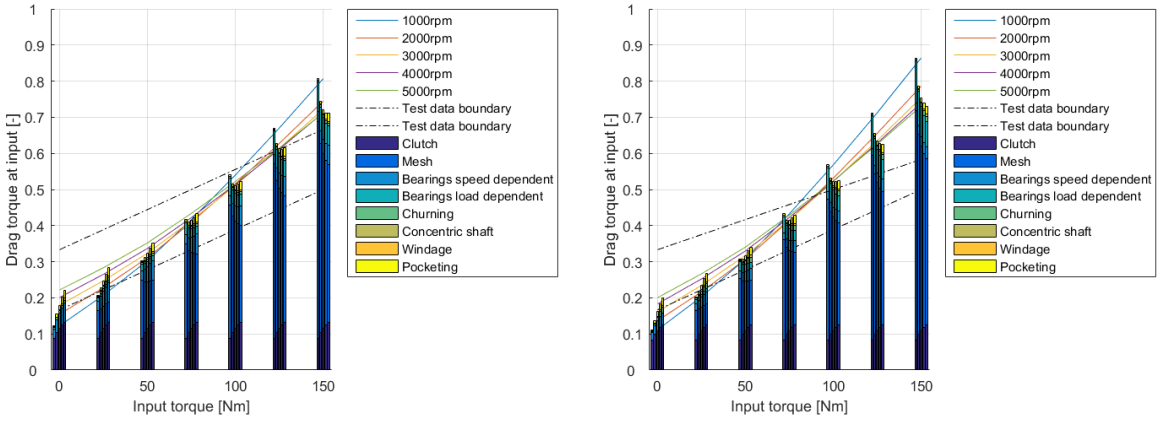

(a) $40°C$ **(b)** $80°C$

Figure 36: Normalized total drag torque in different temperatures in low gear

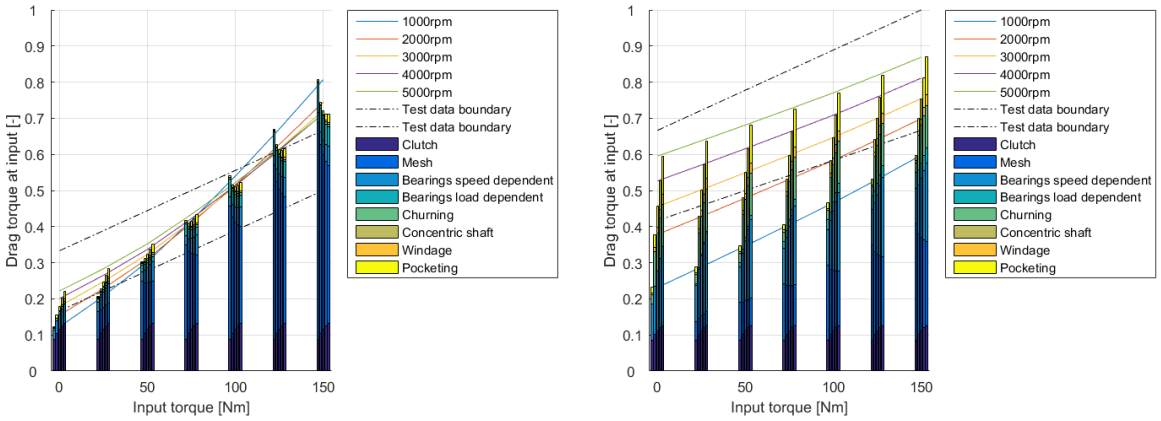

(a) Low gear **(b)** High gear

Figure 37: Normalized total drag torque in different gears at $40°C$

From figures 36 and 37, the total drag drag torque can be seen combined with the lower and upper boundary for test results.
Drag torque from gear mesh is dominating at all operating conditions when in low gear while it stands for a smaller portion when a higher gear is engaged. However, when a higher gear is engaged, the speed-dependent losses grow. Especially pocketing, churning and speed-dependent losses from the bearings make up for big parts in higher gears. It can be seen that in lower gears, the load-dependent losses from bearings stands for 50% or more of the losses from bearings while in higher gears the speed-dependent losses are dominating. When it comes to drag torque from the concentric shafts, it can be seen that it is negligible.
In lower gears and low input torque, higher input speeds results in higher drag torque. As the input torque increases, lower input speeds results in a higher drag torque. In higher gears, the higher speeds always result in higher drag torque regardless of input torque. However, the difference between the input speeds decreases with increased input torque.

3.2 Synchronizer

3.2.1 Current synchronizers

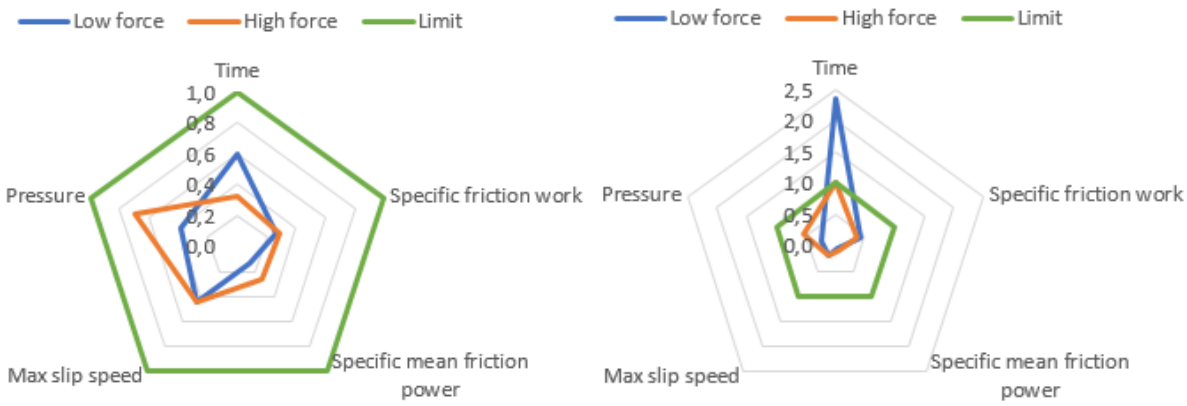

(a) Double up-shift, odd gear **(b)** Double down-shift, odd gear

Figure 38: Normalized limitations for friction lining at $40°C$

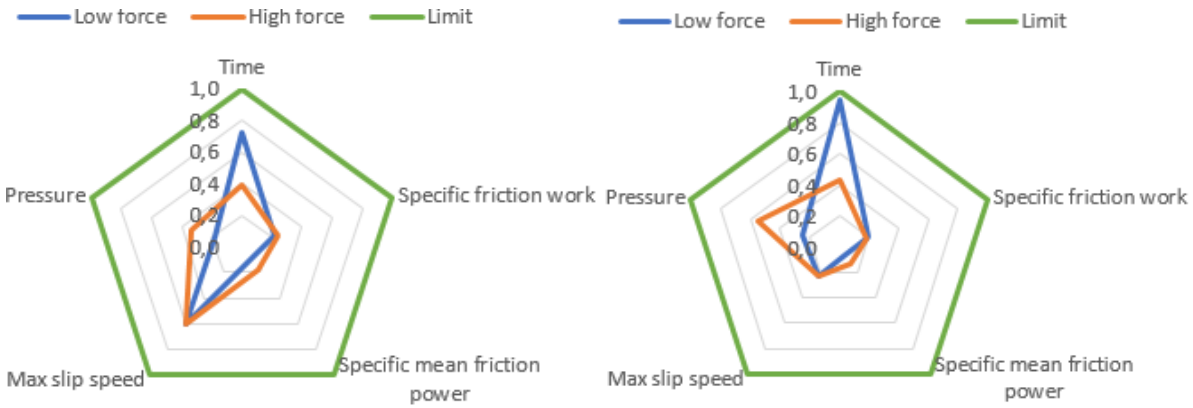

(a) Double up-shift, even gear **(b)** Double down-shift, even gear

Figure 39: Normalized limitations for friction lining at $40°C$

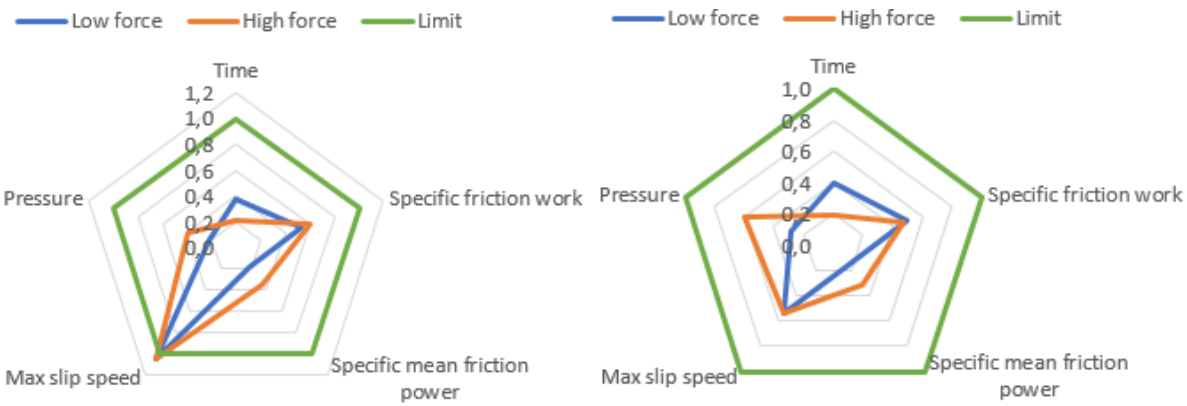

(a) Quadruple up-shift, odd gear

(b) Quadruple down-shift, odd gear

Figure 40: Normalized limitations for friction lining at $40°C$

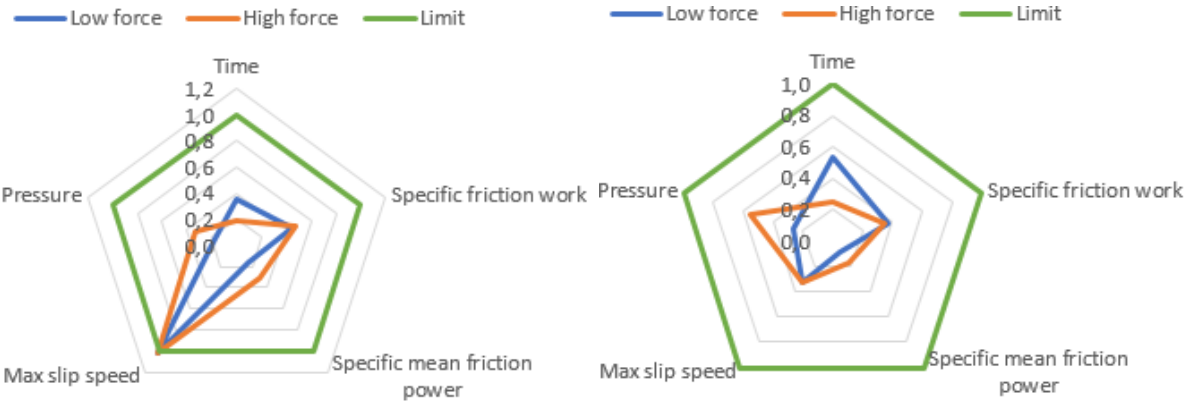

(a) Quadruple up-shift, even gear

(b) Quadruple down-shift, even gear

Figure 41: Normalized limitations for friction lining at $40°C$

Figures 38 to 41 show how the synchronizer performs relative to the specification of the friction lining durability and slip time requirements when a low or high axial force is applied to the synchronizer ring via the sleeve, see section 2.1. The input speed is the maximum of what is allowed according to specification for before up-shifts or after down-shifts.
It can be seen that the friction lining is subjected to conditions it can handle in all cases except when a quadruple up-shift is performed in which slip-speed is out of specifications, see figure 40. The overshooting over permissible speed is then quite small. The other quantities are only above 60% in a one case, double up-shift at odd-gears, and are commonly lower than 50%.
It can also be seen that a higher force always leads to a shorter slipping time. There is only one case in which the slipping time is too high even with the high axial force applied, double down-shift in odd gears.

3.2.2 Synchronizers with inertial changes

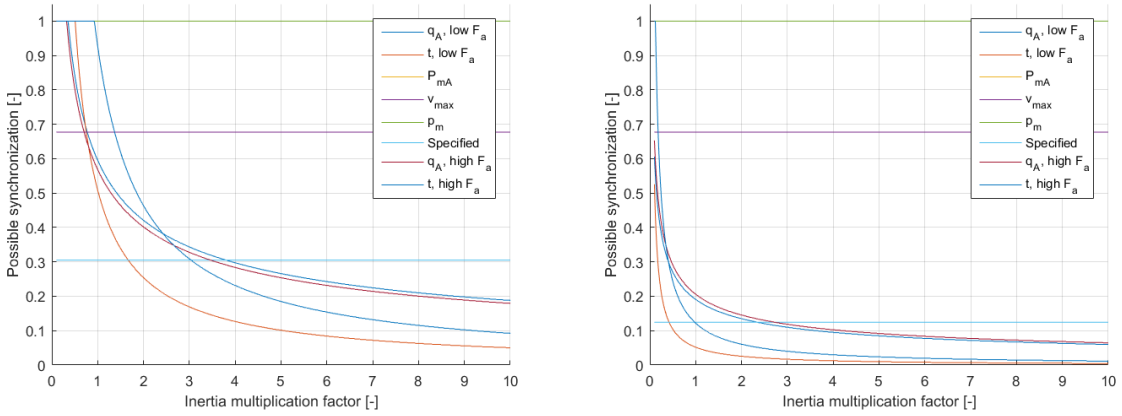

(a) Double up-shift, odd gear **(b)** Double down-shift, odd gear

Figure 42: Normalized limitations for synchronized speed at 40°C

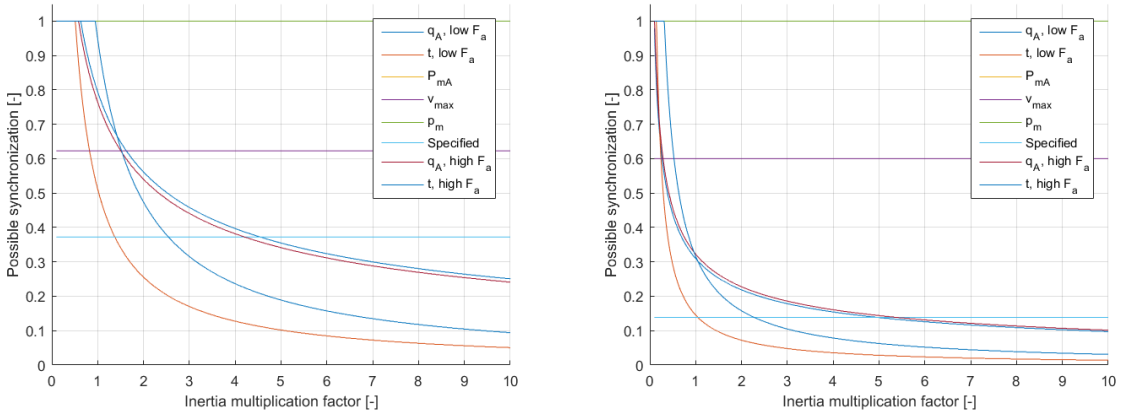

(a) Double up-shift, even gear **(b)** Double down-shift, even gear

Figure 43: Normalized limitations for synchronized speed at 40°C

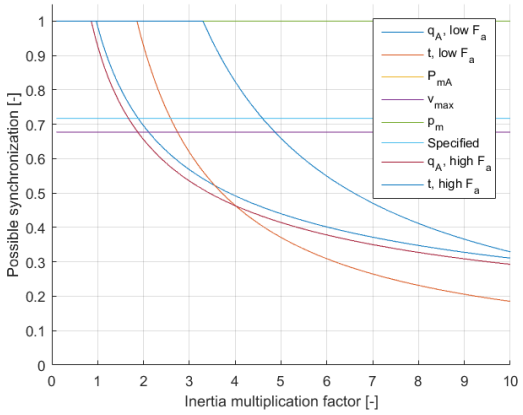

(a) Quadruple up-shift, odd gear

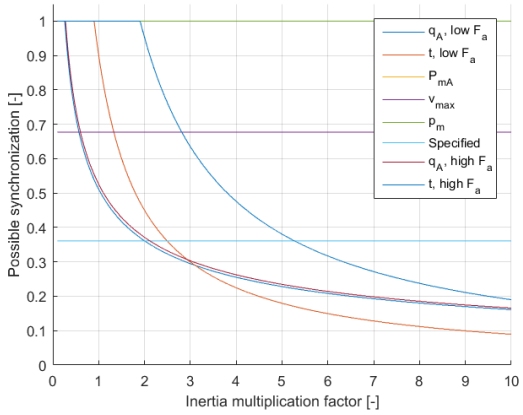

(b) Quadruple down-shift, odd gear

Figure 44: Normalized limitations for synchronized speed at 40°C

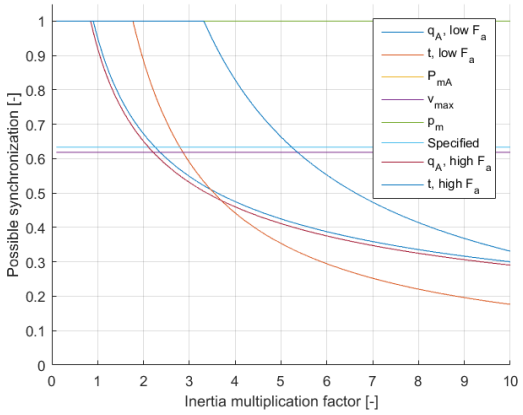

(a) Quadruple up-shift, even gear

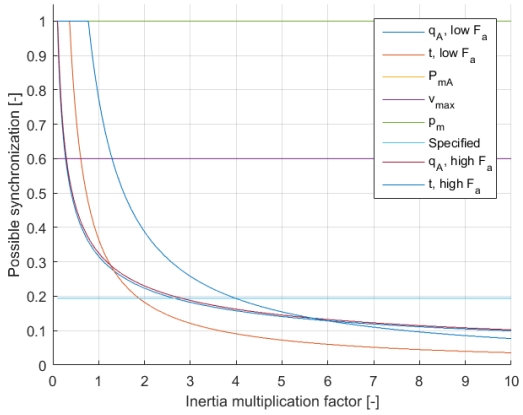

(b) Quadruple down-shift, even gear

Figure 45: Normalized limitations for synchronized speed at 40°C

Figures 42 to 45 show how the inertia influences the allowed speed difference between target gear and output shaft with respect to the four design parameters and the quality parameter. The company specified maximum speed difference for the current transmission is also shown as a reference line, labelled "Specified". The models only evaluates speeds up to 1 revolution speed unit and actual values may be higher. Only the limiting parameter, i.e. the curve closest to the x-axis for each value of x, is of interest.

From figures 42 to 45, it can be seen that only the specific frictional work and the slip time are functions of the reduced inertia that the synchronizer has to overcome (P_{mA} and P_m coincide). The results are in general worse for lower gears and down-shifts compared to higher gears and up-shifts.
To use different forces at the actuator affects specific frictional work slightly and the slip time significantly. Specific frictional work increases with higher force in down-shifts and decreases with higher force in up-shifts. The slip time decreases with higher force in both up- and down-shifts.

4 Discussion

4.1 Drag torque

4.1.1 Bearings

All models for drag torque in bearings are provided with very little information of what they are based on. The SKF model states that it is based on simplified equations of more advanced computational methods [27]. The Schaeffler and ISO models are empirical with no explanation of any physical connection in the equations. It is therefore difficult to explain why there sometimes is such a big difference between the models.

The SKF and Schaeffler models are mostly relatively close to each other except at higher temperatures while the ISO model is constantly some way off. This is probably due to the values of the bearing constants f_1 and f_0. There is no explanation about how these constants are determined but the difference between the constants in the different models is significant.

Another find is that while the Schaeffler and ISO models are strictly growing, the SKF model sometimes has a negative gradient. One possible reason could be that the SKF model considers seals and mentions that they can contribute to a big portion of the drag torque [27] while the other models seem to not consider seals. Since the seals are a speed dependent drag torque it would increase with increased speed as the SKF model does.

The models also show different behaviours when it comes to different temperatures. There are two ways temperature can affect the drag torque in the bearings. First, a higher temperature yields a lower viscosity which lowers the resistance from the oil. Secondly, this lower viscosity might mean that the lubrication suffer and therefore a bigger frictional drag torque is introduced.

A higher gear yields a higher speed which results in higher speed dependent losses since more oil has to be moved per unit of time. All models show this intuitive behaviour.

The hybrid model is chosen to adapt the bearings to their respective manufacturers.

4.1.2 Clutch

The different clutch models show somewhat similar results throughout different operating conditions except for model 2 and 4 when it comes to a high oil flow. This is most likely a result of how the different models treat the centrifugal force. Model 2 and 4 have as a boundary condition that one disc is stationary while the other only has the relative speed as absolute speed. This will not affect the drag torque calculation directly since it is the relative speed between them that determines the viscous shear and therefore the drag torque generated in the clutch. However, it affects the calculation indirectly since with higher absolute rotational velocities on both discs, a greater centrifugal force is generated and therefore there will be less oil to generate drag torque in between the clutch discs.
It should be noted that it has been assumed that the oil flow is split equally into the different clutch gaps. In reality this must not be the case so each interface might have to be modelled individually and summed up. This has not been in the scope of this thesis.

Model 1 and 5 are virtually unaffected by the change in clutch gap while the others decrease slightly, especially in lower speeds. All the models tend towards the same results. This can be explained by that a bigger gap will provide a longer distance for the fluid to shear. With the soap-bubble analogy, the shear stress will decrease with a decrease in gradient. It should however be noted that the same clutch gap is assumed between all interfaces. In reality, there might be a difference here so that each interface has to be modelled individually and summed up. This has not been in the scope of this thesis.

All models show a decrease in drag torque when temperature increases. This is intuitive due to reduced viscosity at higher temperatures and therefore less resistance. There is a difference between the models when it comes to how much they are affected by an increase in temperature. At a higher temperature, they move closer to each other. This might be due to how model 2 and 4 do not consider absolute rotational speeds. Therefore they have more oil in between the discs and are more affected by an increase in oil temperature.

There are two very distinct groups of models when it comes to higher gears. One increases greatly while the other is barely affected. This is most likely also due to how the models treat the speeds and therefore the centrifugal force. Model 1 and 5 even decrease slightly which is probably due to that the increased centrifugal force results in more area with mist and less with oil film between the discs. Also, the relative speed between the clutch discs move closer to zero when higher gears are selected and this also points to the difference between the two distinct group of results.

All models are multiplied with a constant area ratio after calculation. As an assumption, this constant is simply the ratio between non-grooved disc and complete disc. Since the grooves have a finite depth and walls that are perpendicular towards the flow, this assumption might not be accurate.

The difference between model 1 and model 5 is always small. This points to the fact that truncation performed in model 1 was effective and non-intrusive on accuracy.

Model 5 seems to be the most accurate since it considers the rotational velocity of both discs, it considers all regions and it has less of simplification compared to model 1. Model 1 seems to have similar accuracy but the difference in computational resources needed is slim so the truncation is not needed.

4.1.3 Churning

All models except model 2 show a decrease in drag torque with increase in temperature. For model 2, this could be due to the turbulent flow that exists at higher temperatures thereby providing more resistance to the gears, as seen from table 4. For model 1 and 3, it is more intuitive due to the reduced viscosity at higher temperatures and also due to the reason that these model do not consider the flow characteristics of the oil. For model 2, it is seen that the change in oil volume within the transmission does not affect the drag toque significantly and this points to that the churning loss is more dependent on the oil level present in the gearbox and not the volume itself. Churning loss, being a speed dependent loss, will produce higher values at higher speeds as more oil has to be moved per time unit.

In model 1, the churning loss is a function of static oil level which does not represent reality well since effective oil level decreases with increased speed. In model 2, however, the churning loss is determined through dimensional analysis and therefore includes the dynamic oil level at different speeds. The determination of dimensional coefficients in the model, however, is based on experiments conducted by the author on spur gears [5]. This means that the exponents used may not be completely accurate for the transmission being modelled.

Model 3 has two major flaws. First, it simplifies the gear as a smooth shaft and justifies this with that the teeth contribute to a larger diameter. However, with teeth, a surface that is perpendicular, or almost perpendicular, against the flow, is introduced. It seems non-plausible that this perpendicular action between gear and fluid is compensated for with a slightly larger diameter for a smooth surface with only tangential interaction with the fluid. Secondly, the model only considers friction drag and not form drag. This goes well along with the assumption of a smooth surface with only tangential interaction with the fluid. It does however seem unlikely that form drag can be neglected when there are teeth present with a face perpendicular towards the fluid.

Model 2 is used due to its consideration of a dynamic oil level and both gear geometry and lubricant properties.

4.1.4 Concentric shaft

An increase in temperature leads to lower drag torque and this is due to the decrease in the oil viscosity at higher temperatures, which directly influences the drag torque. Also, the drag torque obtained due to concentric shaft shear is very low at all operating conditions. As a result, no additional models to estimate the concentric shaft drag torque have been developed.

The concentric shaft drag torque is a function of relative speed difference between the two input shafts. Based on the experimental data on the relative speeds of the input shafts, the relative speed difference reduces as the gear number increases (with no other gear pre-engaged) and hence this reduction leads to reduced concentric shaft drag torque at higher gears. The relative speed also decreases at very high input speeds. That is why the gradient goes from positive to negative when input speed passes a threshold.

4.1.5 Windage

The windage drag torque seems to be temperature-independent. The current windage model does not consider the fluid properties in the equations and therefore the temperature changes does not influence the drag torque results. This can be explained by that while oil changes its properties greatly with temperature, windage is only affected by air and oil-mist properties.

A higher gear selection results in higher losses which is intuitive.

4.1.6 Pocketing

Pocketing, or squeezing, losses are a speed dependent type of loss and as a result produce higher drag torque at higher speeds. More non-intuitive is that both models show very low dependency on temperature. Maurer's model doesn't depend on temperature or medium properties at all. Mauz's model, however, does consider the density of the fluid and indirectly viscosity through conditions. Mauz's model is therefore used due to taking medium properties in consideration and being the most developed model according to [6]. The results from this model are, however, within the limits for having an uncertainty of 50%. In higher gears, pocketing makes up for a significant part of total drag torque while in lower gears an accuracy this bad might be acceptable.

Both models are of the simpler kind and the high uncertainty combined with non-intuitively low dependency on temperature justifies skepticism towards the results.

4.1.7 Gear mesh

With the highest contribution of drag torque coming from the gear mesh, multiple models were developed to give a better comparison between each other and finally utilize the one that agrees well with one another. But, as seen in the figures 27 to 29, the models produce results that are quite different from each other but follow a similar trend.

All models show that an increase in input torque results in an increase in drag torque. This is intuitive since a higher torque implies greater forces between teeth in the mesh region. Friction is dependent on this force and therefore drag torque increases.

In figure 28, it is seen that higher temperature leads to higher drag torque. In the region between the meshing gear teeth, there exists a very thin film of oil that is being squeezed. At lower temperatures, the oil has high viscosity and hence thicker oil is present between the gears and leading to lower coefficient of friction between the contact surfaces of the meshing gears. As temperature increases, the oil in the gap becomes thinner and therefore provides less lubrication so that contact friction increases, leading to higher frictional resistance.

With an increase in rotational speeds of the gears, the friction between the mating teeth reduces. As engaged gears are increased, the rotational speeds of the gears change depending on the gear ratios and as a result of higher speeds, lower friction is produced between the mating teeth. This results in reduction of drag torque at higher chosen gears when compared to lower chosen gears.

In model 1, there are certain limitations to its utilization like the boundary constraints of the pitch line velocity and the load intensity. If the values are outside the boundary conditions, these need to be determined through experience, which the authors of this thesis lack. In models 2,3 and 4, there exist boundary constraints as well. In these models, values outside the boundary are given the maximum or minimum boundary value based on the location of the value. Model 5 utilizes a constant, C_1, that influences the sliding friction coefficient and this value is based on an experiment conducted by the author of the source and hence, the reliability of this constant also becomes a question.

Since all the models behave in the same way, it can be concluded that the trend is probably correct. However, to choose which model to use, the absolute values have to be considered. This was done through comparison with test data which led to model 2 being chosen. This does, however, not mean that this model is the most physically correct. Since this model scales linearly with a lubrication factor that is unknown (along with model 3 and 4 as well), it can be adjusted to fit the test results. It should also be noted that this exposes a risk that, even though the total drag torque may be close to test data, the distribution between sources of drag torque may be incorrect.

4.1.8 Load-dependent

The decrease in load dependent drag torque with increase in gear or input speed, can be explained through equations 153, 159 and 170. The higher speed simply leads to a lower coefficient of friction. The power loss might be higher depending on the relation between increase in speed and decrease in coefficient of friction, however this paper only handles drag torque and not efficiency.

The increase in load dependent drag torque at a higher temperature can be explained by that the lubricant is more easily moved and therefore less of it is providing lubrication to the contact surfaces in both gears and bearings. Therefore sliding friction increases.

4.1.9 Speed-dependent

Intuitively, the speed dependent drag torque increases with an increase in speed and gear. This is due to that more oil and air has to be moved per unit of time at higher speeds. More counter-intuitively is that temperature has a very small impact. However, if figure 33 is inspected, it can be seen that the oil viscosity has the biggest gradient before 20°C. The viscosity at 80°C is though less than 35% of that at 40°C.

4.1.10 Total

The total results correspond relatively well with the test results given the complexity of the problem investigated. At a low gear it can be seen that gear mesh is the dominant source of drag torque which becomes smaller at higher speeds and higher gear due to decreasing coefficient of friction. An increase

in temperature actually increases drag torque which points towards that the reduced drag torque due to reduced viscosity and therefore speed dependent losses has a smaller effect than the increased sliding friction in gear meshes and bearings due to less lubricant existing between contact surfaces.

4.2 Synchronizers

4.2.1 Current synchronizers

The current synchronizers seem to be over-dimensioned when it comes to frictional powers and work and only fails slightly for slip speed at the extreme condition of quadruple up-shifting at maximum allowed engine speed. This shows that a better understanding of drag torque is needed to better dimension the synchronizers. In order to decrease slip speed and increase frictional powers, a smaller diameter is required on the synchronizers. This can however compromise the solid mechanics of other components.

The axial forces required to push the synchronizers also influence the capabilities of the friction lining within the synchronizers. A higher axial force for the same distance will lead to a higher frictional power and as a result might end up burning out the friction lining if the power is beyond the limit.

4.2.2 Synchronizers with inertial changes

Mainly, respect only has to be given to frictional work and slip time when considering a change in inertia. Slip speed should also be considered at small increases in inertia during quadruple up-shifts. Since maximum engine speeds are defined for each gear before an up-shift and after a down-shift, the slipping speed will stay the same. The limitation from frictional powers are not affected since a higher inertia also generates a longer slip time for the synchronization. These powers are always outside of the domain investigated.

5 Future work

5.1 Bearings

Bearings contributes to a significant part of the total drag torque and there are non-negligible differences between the models. However, it is believed that the manufacturers have provided accurate models and that, for example, the seals can explain differences between them. It is also very complicated to develop models considering all parameters affecting the bearings. Future work should instead be focused on perfecting the coefficients used in the models, since the correct bearing was not always available in the catalogues.

5.2 Clutch

Further work needed since some aspects are not considered in the clutch. Oil flow and clutch gap are unknowns that are difficult to determine, especially if they are unequally split between the interfaces. However, they seem to only have a slight effect on the drag torque. Further work regarding clutch gap and oil flow should have low priority and might be of academic interest only.
The area ratio between grooved and total area, on the other hand, has a big influence. Total drag torque from the clutch scales linearly with this factor, therefore it should be modelled more in detail how the grooves affect the drag torque. The clutch is also a significant part of total drag torque, therefore this should have high priority.

5.3 Churning

Future work could be either to determine the oil level as a function of engaged gear, temperature and input speed so that the ISO model can be utilized. This could be difficult since there is no clearly defined surface in a gearbox when gears are turning in high speed. Considering model 2, an attempt could be made to isolate churning losses and through that conduct a dimensional analysis on the considered gearbox to get more accurate coefficients. This might however prove to be quite a big of an endeavour since there are many gear-combinations, speeds, temperatures and other variables that can influence and therefore have to be investigated. Also, the model will only be applicable to the transmission the experiments are conducted on. If there are design differences, the coefficients are not applicable anymore and the whole process will have to be redone.

5.4 Concentric shaft

No future work is recommended on drag torque from concentric shaft. The authors of this thesis find the theory and assumptions behind model reliable and the contribution to total drag torque is very small so that an eventual big relative error is negligible in total.

5.5 Gear mesh

Future work on drag torque from gear meshing should have high priority. There is a big discrepancy between all models, even though they show similar trends. The gear mesh contributes with the largest part of the drag torque in many operating conditions and therefore errors in the models will influence the total results significantly. Also, all models tried in this thesis have been of the more simpler variant. The models accuracy could be increased through either applying a more advanced model or,

if the trend is found reliable, find an accurate value or expression for the lubrication factor. The last alternative might have problems if other values are altered (such as gear geometry) and therefore a new more advanced model is recommended.

5.6 Windage

Air and oil-vapour are both influenced by temperature and will eventually affect the windage drag torque on all the gears. The existing model does not consider this effect and therefore the results do not show any reliable result (section 3.1.5). Future work would include improving the current model or develop a new model to include the effects of temperature , as an example. Although, considering that the contribution of windage drag torque to the total drag torque is low, this task can be a low priority and dealt with if additional time exists.

5.7 Pocketing

Pocketing has a significant contribution, especially at higher speeds. However, the uncertainty is big and the models tested in this thesis have been of the more simple kind. New, more advanced models should be tested in the future to achieve a better accuracy.

References

[1] Neil E. Anderson and Stuart H. Loewenthal. "Spur-gear-system efficiency at part and full load". In: *NASA Technical Paper* (1980).

[2] Ana Pastor Bedmar. "Synchronization processes and synchronizer mechanisms in manual transmissions: Modelling and simulation of synchronization processes". MA thesis. Göteborg: Chalmers University of Technology, 2013.

[3] R. J. Boness. "Churning losses of discs and gears running partially submerged in oil". In: *Int Power Transmission Gearing Conference* 1 (1989), pp. 355–359.

[4] Earle Buckingham. *Analytical mechanics of gears*. McGraw-Hill Book Co., 1949.

[5] C. Changenet and P. Velex. "A Model for the Prediction of Churning Losses in Geared Transmissions—Preliminary Results". In: *Journal of Mechanical Design* 129 (2007), pp. 128–133.

[6] Franco Concli and Carlo Gorla. "Windage, churning and pocketing power losses of gears: different modeling approaches for different goals". In: *Forsch Ingenieurwes* 80 (2016), pp. 85–99.

[7] P. H. Dawson. "Windage loss in larger high-speed gears". In: *Proceedings of the Institution of Mechanical Engineers IMechE* 198A.1 (1984), pp. 51–59.

[8] A. Diez-Ibarbia, A. Fernandez del Rincon, M. Iglesias, A. de-Juan, P. Garcia, and F. Viadero. "Efficiency Analysis of Spur Gears with a Shifting Profile". In: *Meccanica* 51.3 (2016), pp. 707–723.

[9] Carlos M.C.G. Fernandes, Pedro M.T. Marques, Ramiro C. Martins, and Jorge H.O. Seabra. *Influence of Gear Loss Factor on the Power Loss Prediction*. Tech. rep. Porto: Universidade do Porto, 2015.

[10] *Gears Thermal capacity Part 1: Rating gear drives with thermal equilibrium at 95℃ sump temperature*. Switzerland: International Organization for Standardization, 2001.

[11] *Gears Thermal capacity Part 2: Thermal load-carrying capacity*. Switzerland: International Organization for Standardization, 2001.

[12] H. Hashimoto, S. Wada, and Y. Murayama. "The Performance of a Turbulent-Lubricated Sliding Bearing Subject to Centrifugal Effect". In: *Japanese Society of Mechanical Engineering* 49.446 (1984), pp. 1753–1761.

[13] Li Heyan, Jing Qi, and Ma Biao. "Modeling and Parametric Study on Drag Torque of Wet Clutch". In: *Lecture Notes in Electrical Engineering* (2013).

[14] Shoaib Iqbal, Farid Al-Bender, Bert Pluymers, and Wim Desmet. "Mathematical Model and Experimental Evaluation of Drag Torque in Disengaged Wet Clutches". In: *ISRN Tribology* (2013).

[15] Shoaib Iqbal, Farid Al-Bender, Bert Pluymers, and Wim Desmet. "Model for Predicting Drag Torque in Open Multi-Disks Wet Clutches". In: *Journal of Fluids Engineering* 136.2 (2013).

[16] Dan Johnston. *Drag. [online] Centennialofflight.net. Available at:* [Accessed on 2018/05/23]. URL: `http://centennialofflight.net/essay/Theories_of_Flight/drag/TH4.htm`.

[17] T. von Kármán. "On Laminar and Turbulent Friction". In: *National Advisory Commitee for Aeronatuics* 1.4 (1921).

[18] Y. Kato, T. Murasugi, H. Hirano, and T. Shibayama. "Fuel economy improvement through tribological analysis of the wet clutches and brakes of an automatic transmission". In: *JSAE Convention Proceedings* 934 (1993), pp. 57–60.

[19] Hisanao Kitabayashi, Chen Yu Li, and Henry Hiraki. "Analysis of the Various Factors Affecting Drag Torque in Multiple-Plate Wet Clutches". In: *SAE Technical Paper* 2003-01-1973 (2003). https://doi.org/10.4271/2003-01-1973.

[20] Gisbert Lechner and Harald Naunheimer. *Automotive Transmissions: Fundamentals, Selection, Design and Application*. Stuttgart: Springer, 1999.

[21] Ricardo Miguel Peixoto Machado. "Torque loss in helical gears: Influence of 'low loss' gear design". MA thesis. Porto: Universidade do Porto, 2013.

[22] Jörg Maurer. *Hydraulische Verluste von Stirnradgetrieben bei Umfangsgeschwindigkeiten bis 60 m/s*. Vol. 376. Stuttgart: IMK, 1994.
[23] Wolfgang Mauz. *Hydraulische Verluste von Stirnradgetrieben bei Umfangsgeschwindigkeiten bis 60 m/s*. Vol. 159. Stuttgart: IMK, 1987.
[24] David Mba and Petra Heingartner. "Determining power losses in the helical gear mesh; Case study". In: *Gear Technology* (2005).
[25] Gustav Niemann and Hans Winter. *Maschinenelemente Band 2: Getriebe allgemein, Zahnradgetriebe - Grundlagen, Stirnradgetriebe*. Springer, 1989.
[26] Stephen P. Radzevich. *Dudley's Handbook of Practical Gear Design and Manufacture*. 2nd ed. 2012.
[27] *Rolling Bearings*. SKF. 2016.
[28] *Rolling Bearings Catalogue*. Schaeffler. 2014.
[29] Clemens Schlegel, Andreas Hösl, and Sergej Diel. "Detailed Loss Modelling of Vehicle Gearboxes". In: *Proceedings 7th Modelica Conference,* (2009), pp. 434–443.
[30] Herrmann Schlichting and Klaus Gersten. *Boundary-Layer Theory*. seventh. Bochum: Springer Science & Business Media, 1979.
[31] S. Seetharaman and A. Kahraman. "Load-Independent Spin PowerLosses of a Spur Gear Pair:Model Formulation". In: *Journal of Tribology* 131 (2009).
[32] Maximilian Strebel, Michael Wirth, Hermann Pflaum, and Karstel Stahl. "The drag torque behaviour of Manual transmission synchronizers". In: Dallas, Texas, USA: STLE 70th Annual Meeting and Exhibition, 2015.
[33] Victor Streeter and B. Wylie. *Fluid Mechanics*. 8th edition. McGraw-Hill, 1985.
[34] David Talbot, Ahmet Kahraman, and Satya Seetharaman. "A Helical Gear Pair Pocketing Power Loss Model". In: *Journal of Tribology* 136 (2014).
[35] Dennis P. Townsend. "Lubrication and Cooling for High Speed Gears". In: *NASA Technical Memorandum* (1985).
[36] P. Velex and F. Ville. "An Analytical Approach to Tooth Friction Losses in Spur and Helical Gears—Influence of Profile Modifications". In: *Journal of Mechanical Design* 131 (2009).
[37] Paul D. Walker, Nong Zhang, Ric Tamba, and Simon Fitzgerald. "Simulations of drag torque affecting synchronisers in a dual clutch transmission". In: *Japan Journal of Industrial and Applied Mathematics* 28 (2011), pp. 119–140.
[38] S. Yuan, K. Guo, J. Hu, and Z. Peng. "Study on aeration for disengaged wet clutches using a two-phase flow model". In: *ASME Journal of Fluids Engineering* 132.11 (2010). Article ID 111304.
[39] S. Yuan, Z. Peng, and C. Jing. "Experimental research and mathematical model of drag torque in single-plate wet clutch". In: *Chinese Journal of Mechanical Engineering* 24.1 (2011), pp. 91–97.
[40] Yiqing Yuan, Eysion A. Liu, James Hill, and Qian Zou. "An improved hydrodynamic model for open wet transmission clutches". In: *Journal of Fluids Engineering, Transactions of the ASME* 129 (2007), pp. 333–337.
[41] Xingxing Zhou, Paul Walker, Nong Zhang, Bo Zhu, and Jiageng Ruan. "Numerical and experimental investigation of drag torque in a two-speed dual clutch transmission". In: *Mechanism and Machine Theory* 79 (2014), pp. 46–63.

Appendix A

The first simplification of the Navier-Stokes and the continuity equation are made with the help of boundary conditions and assumptions.

With gravitational forces neglected, there are no body forces, $f_r = 0$. Symmetric flow around z-axis yields $\frac{\partial u_\theta}{\partial \theta} = 0$. For equation 29:

$$\underbrace{\frac{Du_R}{Dt}}_{(*)} - \frac{u_\theta^2}{R} = -\frac{1}{\rho}\frac{\partial p}{\partial R} + \frac{\mu}{\rho}\left(\underbrace{\nabla^2 u_R}_{(**)} - \frac{u_R}{R^2} - \underbrace{\frac{2}{R^2}\frac{\partial u_\theta}{\partial \theta}}_{(***)}\right) \tag{184}$$

where

$$(*): \frac{Du_R}{Dt} = \underbrace{\frac{\partial u_R}{\partial t}}_{\text{=0 due to steady state}} + u_R\frac{u_R}{\partial R} + \frac{u_\theta}{R}\overbrace{\frac{\partial u_R}{\partial \theta}}^{\text{=0 due to symmetric flow}} + \underbrace{u_Z}_{\text{=0 due to no flow along Z}}\frac{\partial u_R}{\partial Z} \tag{185}$$

$$(**): \nabla^2 u_R = \frac{\partial^2 u_R}{\partial R^2} + \frac{1}{R}\frac{\partial u_R}{\partial R} + \frac{1}{R^2}\underbrace{\frac{\partial^2 u_R}{\partial \theta^2}}_{\text{=0 due to symmetric flow around Z}} + \frac{\partial^2 u_R}{\partial Z^2} \tag{186}$$

$$(***) = 0, \text{ due to symmetry around z-axis} \tag{187}$$

which yields

$$u_R\frac{\partial u_R}{R} - \frac{u_\theta^2}{R} = -\frac{1}{\rho}\frac{\partial p}{\partial R} + \frac{\mu}{\rho}\left(\frac{\partial^2 u_R}{\partial R^2} + \frac{1}{R}\frac{\partial u_R}{\partial R} + \frac{\partial^2 u_R}{\partial Z^2} - \frac{u_R}{R^2}\right) \tag{188}$$

With gravitational forces neglected, there are no body forces, $f_\theta = 0$. Symmetric flow around z-axis yields $\frac{\partial u_\theta}{\partial \theta} = 0$. For equation 30:

$$\underbrace{\frac{Du_\theta}{Dt}}_{(*)} + \frac{u_R u_\theta}{R} = -\frac{1}{R\rho}\underbrace{\frac{\partial p}{\partial \theta}}_{(**)} + \frac{\mu}{\rho}\left(\underbrace{\nabla^2 u_\theta}_{(***)} - \frac{u_\theta}{R^2} - \underbrace{\frac{2}{R^2}\frac{\partial u_R}{\partial \theta}}_{(****)}\right) \tag{189}$$

where

$$(*): \frac{Du_\theta}{Dt} = \underbrace{\frac{\partial u_\theta}{\partial t}}_{\text{=0 due to steady state}} + u_R\frac{u_\theta}{\partial r} + \frac{u_\theta}{R}\overbrace{\frac{\partial u_\theta}{\partial \theta}}^{\text{=0 due to symmetric flow}} + \underbrace{u_Z}_{\text{=0 due to no flow along Z}}\frac{\partial u_\theta}{\partial Z} \tag{190}$$

$$(**): \frac{\partial p}{\partial \theta} = 0, \text{ due to symmetry around z-axis} \tag{191}$$

$$(***): \nabla^2 u_\theta = \frac{\partial^2 u_\theta}{\partial R^2} + \frac{1}{R}\frac{\partial u_\theta}{\partial R} + \frac{1}{R^2}\underbrace{\frac{\partial^2 u_\theta}{\partial \theta^2}}_{\text{=0 due to symmetric flow around Z}} + \frac{\partial^2 u_\theta}{\partial Z^2} \tag{192}$$

$$(****) = 0, \text{ due to symmetry around Z-axis} \tag{193}$$

which yields

$$u_R \frac{\partial u_\theta}{\partial R} + \frac{u_R u_\theta}{R} = \frac{\mu}{\rho}\left(\frac{\partial^2 u_\theta}{\partial R^2} + \frac{1}{R}\frac{\partial u_\theta}{\partial R} + \frac{\partial^2 u_\theta}{\partial Z^2} - \frac{u_\theta}{R^2}\right) \tag{194}$$

With gravitational forces neglected, there are no body forces, $f_z = 0$. There is no flow along the Z-axis, $u_Z = 0$. For equation 31:

$$0 = -\frac{\partial p}{\partial Z} \tag{195}$$

With no flow along Z-axis it follows that $\frac{\partial u_Z}{\partial Z} = 0$. Symmetric flow around Z-axis yields $\frac{\partial u_\theta}{\partial \theta} = 0$. Applying the product rule for derivatives, the continuity equation 32 yields:

$$\frac{\partial u_R}{\partial R} + \frac{u_R}{R} = 0 \tag{196}$$

The second simplification of the model is done through truncation according to [15]. The truncation is achieved through normalizing the equations and analyze each terms relative magnitude. The source suggests the following dimensionless variables:

$$V^* = \frac{2\pi R_m h u_R}{Q_a}, \text{ for radial velocity} \tag{197}$$

$$U^* = \frac{u_\theta}{R_m \omega_m}, \text{ for tangential velocity} \tag{198}$$

$$Z^* = \frac{Z}{h}, \text{ axial coordinate} \tag{199}$$

$$R^* = \frac{R}{R_m}, \text{ radial coordinate} \tag{200}$$

$$H^* = \frac{H}{R_m}, \text{ clutch gap} \tag{201}$$

$$Re_r^* = \frac{\rho Q_a h}{2\pi\mu R_m^2}, \text{ Reynold's number in radial direction} \tag{202}$$

$$Re_\theta^* = \frac{2\pi\rho R_m^2 \omega_m^2 h^3}{\mu Q_a}, \text{ Reynold's number in circumferential direction} \tag{203}$$

$$P^* = \frac{2\pi h^3 p}{\mu Q_a}, \text{ pressure} \tag{204}$$

This yields the following dimensionless equations:

$$Re_r^* V^* \frac{\partial V^*}{\partial R^*} - Re_\theta^* \frac{U^{*2}}{R^*} = -\frac{\partial P^*}{\partial R^*} + \frac{\partial^2 V^*}{\partial Z^{*2}} + H^{*2}\left(\frac{\partial^2 V^*}{\partial R^{*2}} + \frac{1}{R^*}\frac{\partial V^*}{\partial R^*} - \frac{V^*}{R^{*2}}\right) \tag{205}$$

$$Re_r^*\left(V^*\frac{\partial U^*}{\partial R^*} + \frac{V^* U^*}{R^*}\right) = \frac{\partial^2 U^*}{\partial Z^{*2}} + H^{*2}\left(\frac{\partial^2 U^*}{\partial R^{*2}} + \frac{1}{R^*}\frac{\partial U^*}{\partial R^*} - \frac{U^*}{R^{*2}}\right) \tag{206}$$

instead of equation 188 and 194. In the case of the studied clutch at a load case at 80℃ and a low or high flow rate, H and Re_r are always «1 while Re_θ is always >100. At a temperature of 20℃, Re_r are always «1 while Re_θ is always >5. The ratio is always above 100. Therefore, all terms including Re_r or H can be eliminated without unacceptable loss of accuracy. Final equations:

$$\frac{\partial u_R}{\partial R} + \frac{u_R}{R} = 0 \tag{207}$$

$$-\frac{u_\theta^2}{R} = -\frac{1}{\rho}\frac{\partial p}{\partial R} + \frac{\mu}{\rho}\frac{\partial^2 u_R}{\partial Z^2} \tag{208}$$

$$0 = \frac{\mu}{\rho}\frac{\partial^2 u_\theta}{\partial Z^2} \tag{209}$$

$$0 = -\frac{\partial p}{\partial Z} \tag{210}$$

To solve the equations, equation 209 is integrated twice:

$$\int\int \frac{\mu}{\rho}\frac{\partial^2 u_\theta}{\partial Z^2} dZ dZ = \int\int 0 dZ dZ \tag{211}$$

$$\frac{\mu}{\rho}\int \frac{\partial u_\theta}{\partial Z} dZ = \int C_1 dZ \tag{212}$$

$$\frac{\mu}{\rho} u_\theta = C_1 Z + C_2 \tag{213}$$

$$\implies \quad u_\theta(R,\theta,Z) = \frac{\rho}{\mu}(C_1 Z + C_2) \tag{214}$$

Applying boundary conditions from 28:

$$u_\theta(R,\theta,0) = R\omega_1 \implies \frac{\rho}{\mu}(0 + C_2) = R\omega_1 \implies C_2 = \frac{\mu}{\rho} R\omega_1 \tag{215}$$

$$u_\theta(R,\theta,h) = R\omega_2 \implies \frac{\rho}{\mu}(C_1 h + \frac{\mu}{\rho} R\omega_1) = R\omega_2 \implies C_1 = \frac{\frac{\mu}{\rho}(R\omega_2 - R\omega_1)}{h} \tag{216}$$

$$\implies u_\theta = R\left((\omega_2 - \omega_1)\frac{Z}{h} + \omega_1\right) \tag{217}$$

Insert into 208, rearrange and develop:

$$\frac{\partial^2 u_R}{\partial Z^2} = \frac{1}{\mu}\frac{\partial p}{\partial R} - \frac{\rho R}{\mu}\left(\underbrace{(\omega_2 - \omega_1)}_{\Delta\omega}\frac{Z}{h} + \omega_1\right)^2 = \frac{1}{\mu}\frac{\partial p}{\partial R} - \frac{\rho R}{\mu}\left(\Delta\omega^2\frac{Z^2}{h^2} + 2\Delta\omega\omega_1\frac{Z}{h} + \omega_1^2\right) \tag{218}$$

Integrating twice:

$$\int\int \frac{\partial^2 u_R}{\partial Z^2} dz dz = \int\int \frac{1}{\mu}\frac{\partial p}{\partial R} - \frac{\rho R}{\mu}\left(\Delta\omega^2\frac{Z^2}{h^2} + 2\Delta\omega\omega_1\frac{Z}{h} + \omega_1^2\right) dZ dZ \tag{219}$$

$$\implies \int \frac{\partial u_R}{\partial Z} dZ = \int \frac{1}{\mu}\frac{\partial p}{\partial R} Z - \frac{\rho R}{\mu}\left(\Delta\omega^2\frac{Z^3}{3h^2} + \Delta\omega\omega_1\frac{Z^2}{h} + \omega_1^2 Z\right) + C_1 dZ \tag{220}$$

$$\implies u_R(R,\theta,Z) = \frac{1}{2\mu}\frac{\partial p}{\partial R} Z^2 - \frac{\rho R}{\mu}\left(\Delta\omega^2\frac{Z^4}{12h^2} + \Delta\omega\omega_1\frac{Z^3}{3h} + \omega_1^2\frac{Z^2}{2}\right) + C_1 Z + C_2 \tag{221}$$

Applying boundary conditions from 27:

$$u_R(R,\theta,0) = 0 \implies C_2 = 0 \tag{222}$$

$$u_R(Z,\theta,h) = 0 \implies C_1 = -\frac{1}{2\mu}\frac{\partial p}{\partial R} h + \frac{\rho R}{\mu}\left(\Delta\omega^2\frac{h}{12} + \Delta\omega\omega_1\frac{h}{3} + \omega_1^2\frac{h}{2}\right) \tag{223}$$

which finally yields the radial velocity:

$$u_R = \frac{1}{2\mu}\frac{\partial p}{\partial R}(Z^2 - Zh) - \frac{\rho R}{12\mu h^2}\left(\Delta\omega^2 Z(Z^3 - h^3) + 4\Delta\omega\omega_1 Zh(Z^2 - h^2) + 6\omega_1^2 Zh^2(Z - h)\right) \tag{224}$$

Now the radial flow can be calculated by integrating velocity over area:

$$Q_a = \int_0^{2\pi} \int_0^h u_R R dh d\theta \tag{225}$$

With derived radial velocity:

$$Q_a = -\frac{\pi R h^3}{6\mu} \frac{dp}{dR} + \frac{\rho \pi R^2 h^3}{6\mu} \left(\omega_1^2 + \omega_1 \Delta\omega + \frac{3}{10} \Delta\omega^2 \right) \tag{226}$$

Appendix B

Clutch model 2 has the same derivation as clutch model 1 up to 188, 194, 195 and 196. After that, while model 1 applies truncation for further simplification, model 2 simplifies algebraically. Deriving 196 with regards to R:

$$\frac{\partial}{\partial R}\left(\frac{\partial u_R}{\partial R}+\frac{u_R}{R}\right)=0 \tag{227}$$

Applying the quotient rule:

$$\implies \frac{\partial^2 u_R}{\partial R^2}+\frac{\frac{\partial u_R}{\partial R}R-u_R}{R^2}=0 \tag{228}$$

$$\implies \frac{\partial^2 u_R}{\partial R^2}=-\frac{1}{R}\frac{\partial u_R}{\partial R}+\frac{u_R}{R^2} \tag{229}$$

Inserting into 188:

$$u_R\frac{\partial u_R}{R}-\frac{u_\theta^2}{R}=-\frac{1}{\rho}\frac{\partial p}{\partial R}+\frac{\mu}{\rho}\left(-\frac{1}{R}\frac{\partial u_R}{\partial R}+\frac{u_R^2}{R^2}+\frac{1}{R}\frac{\partial u_R}{\partial R}+\frac{\partial^2 u_R}{\partial Z^2}-\frac{u_R}{R^2}\right) \tag{230}$$

$$\implies u_R\frac{\partial u_R}{R}-\frac{u_\theta^2}{R}=-\frac{1}{\rho}\frac{\partial p}{\partial R}+\frac{\mu}{\rho}\frac{\partial u_R^2}{\partial Z^2} \tag{231}$$

If u_θ is analyzed at the two Z-coordinates $Z=0$ and $Z=h$, it can be derived from the no-slip boundary conditions, 51, that it must be linearly dependent on R. Thus:

$$\frac{\partial^2 u_\theta}{\partial R^2}=0 \tag{232}$$

$$\frac{1}{R}\frac{\partial u_\theta}{\partial R}=\frac{u_\theta}{R^2} \tag{233}$$

$$\implies \frac{\partial u_\theta}{\partial R}=\frac{u_\theta}{R} \tag{234}$$

Inserted in 194 yields:

$$\frac{\partial^2 u_\theta}{\partial Z^2}=0 \tag{235}$$

In analogy with Appendix A, this yields 214. This model does however have different boundary conditions, 51, yielding a different result:

$$u_\theta=R\Delta\omega\frac{Z}{h} \tag{236}$$

$$\implies \frac{u_\theta^2}{R}=R\Delta\omega^2\frac{Z^2}{h^2} \tag{237}$$

Inserted into 231:

$$\implies u_R\frac{\partial u_R}{\partial R}-R\Delta\omega^2\frac{Z^2}{h^2}=-\frac{1}{\rho}\frac{\partial p}{\partial R}+\frac{\mu}{\rho}\frac{\partial^2 u_R}{\partial Z^2} \tag{238}$$

This yields the pressure field:

$$\frac{\partial p}{\partial R}=\frac{27\rho Q^2}{70\pi^2 h_i R^3}+\frac{3\rho\Delta\omega^2 R}{10}-\frac{6\mu Q}{\pi R h_i^3} \tag{239}$$